Lecture 5: Measurements without contact in heat transfer: principles, implementation and pitfalls

JC Krapez[1], H. Pron[2]

[1] ONERA, Salon de Provence, France
 E-mail: krapez@onera.fr
[2] **Université de Reims / GRESPI EA 4694, Reims**
 E-mail: herve.pron@univ-reims.fr

Abstract. The main objective of this lecture is to make the end users aware of the various physical phenomena and especially of the errors frequently met during temperature and heat flow measurement. Phenomena which occur in thermometry without contact (pyrometry with single, two colors or multiwavelength) will be presented. Specificities of radiative methods and procedures to overcome bias in temperature measurement will be discussed. The amount of thermal radiation emitted by a surface is only a fraction of the blackbody radiation at the same temperature. This ratio, i.e. the emissivity, is an additional unknown parameter. Whatever the number of considered wavelengths in passive radiation thermometry, one faces an underdetermined problem, notwithstanding the fact that the atmosphere between the sensed surface and the sensor introduces itself additional unknown parameters. We will present several solutions (and some pitfalls) for the problem of emissivity and temperature separation developed in the field of multiwavelength pyrometry (MWP) and in the field of multiwavelength/hyperspectral remote sensing of earth. Last but not least, a paragraph is especially dedicated to infrared thermography, as far as the technical limitations may have a great influence on both validity and accuracy of the results issued from a parameters estimation procedure.

1. Basic relations for the measured radiance

1.1. Blackbody radiance

Matter spontaneously emits electromagnetic radiation in a very broad spectrum comprising UV, visible light, infrared (IR) and microwaves. The emitted radiance from a surface in a given direction depends on wavelength, on temperature, on direction and also on the considered matter. For a solid material it also depends on the surface state: roughness , presence of corrosion. The maximum emitted radiance at a given wavelength, temperature, and direction is described by the Planck's law (blackbody radiance) [1].

$$B(\lambda,T) = \frac{C_1}{\lambda^5}\left[\exp\left(\frac{C_2}{\lambda T}\right) - 1\right]^{-1}$$

(5.1)

$B(\lambda,T)$ is expressed in W/m^3/sr, wavelength λ in m, temperature T in K, with C_1 = 1.191·10^{-16} W·m^2 and C_2 = 1.439·10^{-2} m·K. The spectral blackbody radiance is described in figure 5.1 for different temperature levels. The maximum emission is observed at a wavelength λ_{max} such that $\lambda_{max}T = 2898\,\mu mK$ (Wien's displacement law). This law tells us that the peak emissive intensity shifts to shorter wavelengths as temperature rises, in inverse proportion to T.
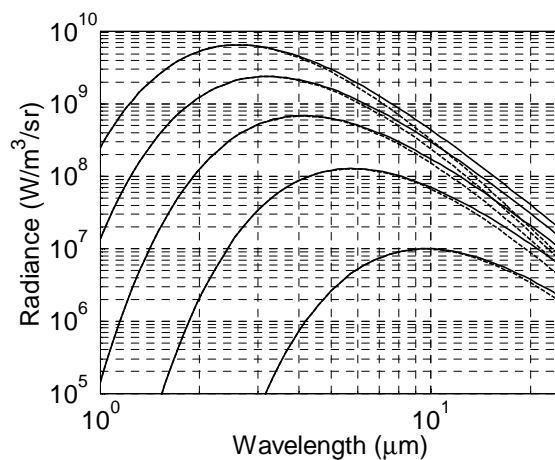

Figure 5.1. Blackbody radiance vs. wavelength for T=300K, 500K, 700K, 900K and 1100K (from bottom to top). Planck's law in continuous line, Wien's law in dashed line.

A common approximation to the Plank's law is the Wien's law, which is also plotted in figure 5.1:

$$B_W(\lambda,T) = \frac{C_1}{\lambda^5}\exp\left(-\frac{C_2}{\lambda T}\right)$$

(5.2)

The approximation error increases with wavelength. One can however consider that the Wien approximation is valid in the rising part of the radiance curve. As a matter of fact the error is less than 1% provided $\lambda T < 3124\,\mu mK$.

It is obvious that by measuring the thermal radiation emitted by the blackbody surface at a given wavelength one could infer its temperature from the Planck's law. This idea is at the origin of pyrometry, thermography, and microwave radiometry.

The sensitivity of blackbody radiance to temperature, according to Planck's law, is plotted in figure 5.2. Figure 5.2-left refers to the absolute sensitivity $\partial B/\partial T$ whereas figure 5.2-right refers to the relative sensitivity $B^{-1}\partial B/\partial T$. The absolute sensitivity presents a maximum at a wavelength $\lambda_{S\,max}$ such that $\lambda_{S\,max}T = 2410\,\mu mK$. For a blackbody at 300K, the maximum

radiance is observed at $\lambda_{\max} = 9.65 \, \mu m$; however the maximum sensitivity to temperature variations is observed at a shorter wavelength, namely $\lambda_{S \max} = 8.03 \, \mu m$. On the other hand, the *relative* sensitivity is continuously decreasing (see figure 5.2-right). The trend is like $1/\lambda$ at short wavelengths. The decreasing nature of relative sensitivity would thus favour short wavelengths for temperature measurement. However the radiance to noise ratio progressively decreases in the meantime. Actually, one should consider all three aspects: the radiance level, the absolute sensitivity and the relative sensitivity, together with the spectral detectivity and thus the signal to noise ratio of the potential sensors, when selecting a wavelength or a spectral band for temperature measurement.
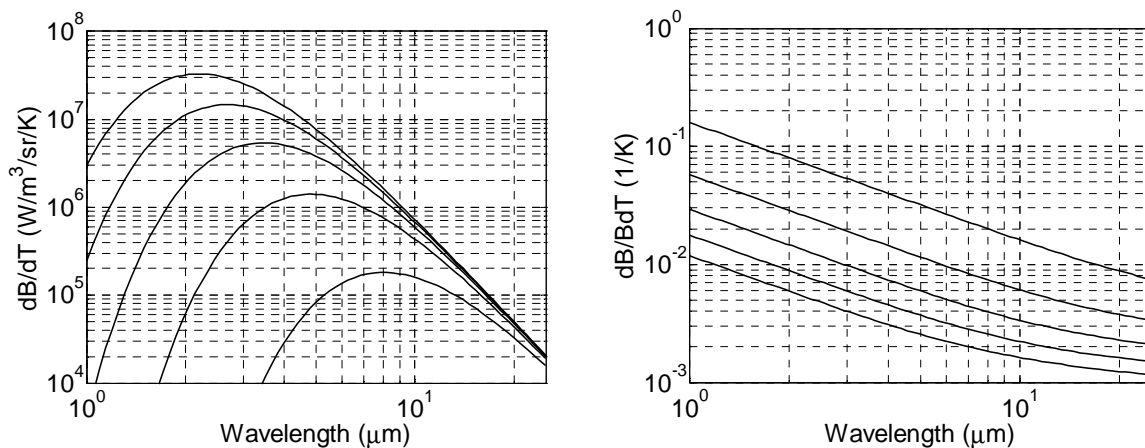

Figure 5.2.   Absolute (left) and relative (right) sensitivity of blackbody radiance to temperature for T=300K, 500K, 700K, 900K and 1100K (resp. from bottom to top and top to bottom).

1.2.   Emissivity and related radiative parameters

The ratio between $L(\lambda, T, \theta, \varphi)$, the radiance effectively emitted by a surface in the direction (θ, φ), and the blackbody radiance $B(\lambda, T)$ at same wavelength and same temperature is called the emissivity:

$$\varepsilon(\lambda, T, \theta, \varphi) = L(\lambda, T, \theta, \varphi)/B(\lambda, T) \leq 1 \qquad (5.3)$$

The emissivity generally depends on the surface temperature too but, just for convenience, we will drop the T dependency.

From the analysis of the radiation in an enclosure one can state the following relation between the emissivity and the hemispherical directional reflectance (for isotropic radiance) [1]:

$$\varepsilon(\lambda, \theta, \varphi) + \rho^{\cap'}(\lambda, \theta, \varphi) = 1 \qquad (5.4)$$

Also, the energy conservation law for an opaque material tells that the energy that is not absorbed by the surface is reflected in all directions. It leads to the following relation between the absorptivity and the directional hemispherical reflectance:

Lecture 5: Measurements without contact in heat transfer: page 3

$$\alpha(\lambda,\theta,\varphi) + \rho^{'\cap}(\lambda,\theta,\varphi) = 1 \tag{5.5}$$

Helmoltz reciprocity principle leads to (for isotropic radiance):
$$\rho^{\cap'}(\lambda,\theta,\varphi) = \rho^{'\cap}(\lambda,\theta,\varphi) \tag{5.6}$$
which, from eq. (5.4) and (5.5), leads itself to the second Kirchhoff's law stating that the spectral emissivity in a given direction (θ,φ) is equal to the spectral absorptivity in the same direction:

$$\varepsilon(\lambda,\theta,\varphi) = \alpha(\lambda,\theta,\varphi) \tag{5.7}$$

The radiation that leaves the surface $L(\lambda,T,\theta,\varphi)$ is the sum of the radiation emitted by the surface and the reflection by the surface of the radiation coming from the environment in all incident directions (θ_i,φ_i) of the upper hemisphere (in this course, without loss of generality, we will generally consider that the surface is facing up):

$$L(\lambda,T,\theta,\varphi) = \varepsilon(\lambda,\theta,\varphi)B(\lambda,T) + \int_{2\pi} \rho^{''}(\lambda,\theta,\varphi,\theta_i,\varphi_i)L^{\downarrow}(\lambda,\theta_i,\varphi_i)\cos\theta_i d\Omega_i \tag{5.8}$$

where $\rho^{''}(\lambda,\theta,\varphi,\theta_i,\varphi_i)$ is the bidirectional reflectance.
Let us now consider temperature measurement with an optical sensor in the direction (θ,φ). The radiance received by the sensor $L_s(\lambda,T,\theta,\varphi)$ includes both the radiance leaving the monitored surface and transmitted along the optical path and the radiance self-emitted by the atmosphere and the optics along this path, $L^{\uparrow}(\lambda,\theta,\varphi)$:

$$L_s(\lambda,T,\theta,\varphi) = \tau(\lambda,\theta,\varphi)L(\lambda,T,\theta,\varphi) + L^{\uparrow}(\lambda,\theta,\varphi) \tag{5.9}$$

where $\tau(\lambda,\theta,\varphi)$ is the transmission coefficient through the air and the collecting optics.
After proper calibration, i.e with a blackbody brought close to the sensor, one can get rid of the contributions of the optics. After that, $\tau(\lambda,\theta,\varphi)$ and $L^{\uparrow}(\lambda,\theta,\varphi)$ are merely relevant of the atmosphere along the optical path.

1.3.   Simplifications of the radiative equation

The general radiation thermometry equation is:
$$L_s(\lambda,T,\theta,\varphi) = \tau(\lambda,\theta,\varphi)\left[\varepsilon(\lambda,\theta,\varphi)B(\lambda,T) + \int_{2\pi} \rho^{''}(\lambda,\theta,\varphi,\theta_i,\varphi_i)L^{\downarrow}(\lambda,\theta_i,\varphi_i)\cos\theta_i d\Omega_i\right] \\ + L^{\uparrow}(\lambda,\theta,\varphi) \tag{5.10}$$

The objective is to evaluate the surface temperature from it. At this point one has to deal with several unknowns: the transmissivity $\tau(\lambda,\theta,\varphi)$ and the self-emission of the atmosphere $L^{\uparrow}(\lambda,\theta,\varphi)$ along the line of sight, the hemispherical environmental radiance $L^{\downarrow}(\lambda,\theta_i,\varphi_i)$, the

bidirectional reflectance $\rho''(\lambda,\theta,\varphi,\theta_i,\varphi_i)$ for all incident directions (θ_i,φ_i) and the directional emissivity $\varepsilon(\lambda,\theta,\varphi)$. Only when all these parameters are determined can we expect getting the blackbody radiance $B(\lambda,T)$ and then the temperature from the measured radiance $L_s(\lambda,T,\theta,\varphi)$.

One common approximation is to consider that the surface is Lambertian, i.e. its optical properties are direction-independent. Equation (5.10) is then simplified as follows:

$$L(\lambda,T)=\varepsilon(\lambda)B(\lambda,T)+(1-\varepsilon(\lambda))L^{\downarrow}(\lambda) \tag{5.11}$$

where $L^{\downarrow}(\lambda,T)$ is the mean (i.e. isotropic equivalent) environment radiance:

$$L^{\downarrow}(\lambda,T)=\frac{1}{\pi}\int_{2\pi}L^{\downarrow}(\lambda,\theta_i,\varphi_i)\cos\theta_i d\Omega_i \tag{5.12}$$

One has access to the spectral at-sensor radiance:

$$L_s(\lambda,T,\theta,\varphi)=\tau(\lambda,\theta,\varphi)\left[\varepsilon(\lambda)B(\lambda,T)+(1-\varepsilon(\lambda))L^{\downarrow}(\lambda)\right]+L^{\uparrow}(\lambda,\theta,\varphi) \tag{5.13}$$

Generally speaking, when dealing with radiative temperature measurement, one faces two problems:
-   the influence of the environment through reflections as well as along-the-path self-emission and attenuation;
-   the *emissivity and temperature separation* problem.

The atmosphere contribution through attenuation and self-emission is particularly relevant when the measurement is performed from large distances as for example in airborne and satellite remote sensing. Specific methods for atmosphere correction were developed for these applications. Emissivity and temperature separation methods that take advantage of the presence of the atmosphere where also devised and we refer the reader to [2] for a review.

For the remaining of this presentation we will assume that an atmosphere correction was implemented and that one has access to the surface-leaving radiance in eq. (5.8) or its counterpart valid for Lambertian surfaces in eq. (5.11).

The next step is to get rid of the reflected radiation $\int_{2\pi}\rho''(\lambda,\theta,\varphi,\theta_i,\varphi_i)L^{\downarrow}(\lambda,\theta_i,\varphi_i)\cos\theta_i d\Omega_i$ or, for lambertian surfaces, $(1-\varepsilon(\lambda))L^{\downarrow}(\lambda)$.

The photothermal approach is an efficient method for this purpose [3], [4]. It requires the use of an additional radiative heat source able to slightly heat up the tested material, like a laser beam. The laser is either pulsed or modulated. Two pyrometers are used at two wavelengths for measuring the spectral radiance slight increase, respectively the radiance modulation. In both cases the useful spectral signals are deprived from the spurious reflections contribution. They are in fact proportional to $\varepsilon(\lambda)\partial B/\partial T(\lambda,T)$; they are then processed like in two-color pyrometry (see § 3), where the two spectral blackbody radiances $B(\lambda_1,T)$ and $B(\lambda_2,T)$ in eq. (5.17) are replaced by the temperature derivatives $\partial B/\partial T(\lambda_1,T)$ and $\partial B/\partial T(\lambda_2,T)$.

The remaining will deal with cases where the most important contribution to the sensed signal is the surface self-emitted radiation. Pyrometry of high temperature surfaces with (relatively) cold surrounding surfaces is a typical example of such cases. After a proper calibration of the optic instrument at each wavelength, one has access to the emitted radiance itself:

$$L(\lambda,T,\theta,\varphi) = \varepsilon(\lambda,\theta,\varphi)B(\lambda,T) \qquad (5.14)$$

It is clear from this relation that an evaluation of the emissivity is necessary to get the temperature. An indirect approach consists in measuring the directional hemispherical reflectance and using equation (5.4), (5.5) and (5.6) to infer the directional emissivity. This requires using an additional radiation source and bringing close to the characterized surface an integrating hemisphere to collect all the reflected radiation. This approach was used to build several databases which give some hints on the emissivity range and spectral variations for specific materials (see for example [5], [6], [7]).
The indirect reflectance approach will not be dealt in this presentation. We will rather review the approaches which consist in *simultaneously* evaluating temperature and emissivity, or which manage to get rid of emissivity in the temperature measurement procedure.
In the field of pyrometry, different methods were devised depending on the number of wavelengths or wavebands used for the measurement: monochromatic (§ 3), bispectral (§ 4), and multiwavelength pyrometry (§ 5).

2. Single-Color Pyrometry

In single color pyrometry one measures, in a given direction, the spectral radiance expressed in equation (5.14). Actually, the raw signal also includes a multiplicative coefficient and an additive coefficient (assuming linearity between radiance and recorded signal). However, by calibrating the sensor with a blackbody at two temperature levels one can get rid of both coefficients. From now on it is considered that this calibration has been applied.
An estimation of the surface emissivity then allows inferring its temperature. This estimation can be based on prior reflectance measurements or it can be extracted from databases. The question is then: what is the consequence of an emissivity error on the temperature evaluation?
By differentiating equation (5.14) one can evaluate the sensitivity of temperature to an error on emissivity:

$$\frac{dT}{T} = -\left(\frac{T}{B}\frac{dB}{dT}\right)^{-1}\frac{d\varepsilon}{\varepsilon} \qquad (5.15)$$

The amplification factor $\left(\dfrac{T}{B}\dfrac{dB}{dT}\right)^{-1}$ can be easily deduced from the relative sensitivity $\dfrac{1}{B}\dfrac{dB}{dT}$ drawn in figure 5.2.
Also, with the Wien's approximation, equation (5.15) reduces to:

$$\frac{dT}{T} = -\frac{\lambda T}{C_2}\frac{d\varepsilon}{\varepsilon}$$

(5.16)

The amplification factor is about 0.08 for a temperature of 1100K and at 1µm. It reaches about 0.2 for a temperature of 300K and at 10µm. A 10% underestimation of emissivity will thus lead to a 0.8% overestimation of temperature in the first case (i.e. 8K) and a 2% overestimation in the second case (i.e. 6K). The advantage of working at short wavelength is evident from this perspective. As a matter of fact, as seen in eq. (5.16) the error amplification is proportional to λ. For this reason some authors recommended to apply pyrometry in the visible spectrum or even in the UV spectrum (see for example [8], [9], [10]). However, although a given emissivity relative error has a lower impact on temperature evaluation at short wavelength, it should not occult the fact that a reasonable estimation of emissivity is nevertheless needed. The retrieved temperature is unavoidably affected by this emissivity estimation [11]. Apart from this, at short wavelength, both the signal and its *absolute* sensitivity to temperature decrease. The choice of the spectral range for pyrometry is thus always a compromise.

3. Two-Color Pyrometry

By performing a measurement at another wavelength, one adds new information, but unfortunately, one also adds a new unknown, namely the spectral emissivity at this supplementary wavelength:

$$\begin{cases} S_1 = L(\lambda_1,T) = \varepsilon(\lambda_1)B(\lambda_1,T) \\ S_2 = L(\lambda_2,T) = \varepsilon(\lambda_2)B(\lambda_2,T) \end{cases}$$

(5.17)

The most popular method consists in calculating the ratio of the two spectral signals:

$$R_{12} = \frac{S_1}{S_2} = \frac{\varepsilon(\lambda_1)}{\varepsilon(\lambda_2)}\frac{B(\lambda_1,T)}{B(\lambda_2,T)} = \frac{\varepsilon(\lambda_1)}{\varepsilon(\lambda_2)}\left(\frac{\lambda_2}{\lambda_1}\right)^5\frac{\exp(C_2/\lambda_2 T)-1}{\exp(C_2/\lambda_1 T)-1}$$

(5.18)

which gives, with the Wien's approximation :

$$R_{12} \approx \frac{\varepsilon(\lambda_1)}{\varepsilon(\lambda_2)}\left(\frac{\lambda_2}{\lambda_1}\right)^5\exp(-C_2/\lambda_{12}T) = \frac{\varepsilon(\lambda_1)}{\varepsilon(\lambda_2)}\left(\frac{\lambda_2}{\lambda_1}\lambda_{12}\right)^5\frac{1}{C_1}B_W(\lambda_{12},T)$$

(5.19)

where the equivalent wavelength λ_{12} of the two-color sensor is defined by :

$$\lambda_{12}^{-1} = \lambda_1^{-1} - \lambda_2^{-1} \quad \Rightarrow \quad \lambda_{12} = \frac{\lambda_1\lambda_2}{\lambda_2-\lambda_1}$$

(5.20)

Ratio two-color pyrometry thus requires knowing the emissivity ratio $\varepsilon(\lambda_1)/\varepsilon(\lambda_2)$ in order to infer temperature from the radiance ratio R_{12} according to equation (5.18) or according to its approximation, equation (5.19). One common assumption is : $\varepsilon(\lambda_1) = \varepsilon(\lambda_2)$ (it is abusively called the *greybody* assumption even though only the two emissivity values at λ_1 and at λ_2 are required to be equal).

Like for one-color pyrometry, it is easy to relate the temperature estimation error to the emissivity error:

$$\frac{dT}{T} = -\frac{\lambda_{12}T}{C_2}\left(\frac{d\varepsilon_1}{\varepsilon_1} - \frac{d\varepsilon_2}{\varepsilon_2}\right) \tag{5.21}$$

Considering the following examples: [T =1100K, $\lambda_1 = 1$µm, $\lambda_2 = 1.5$µm] for the first one, and [T =300K, $\lambda_1 = 10$µm, $\lambda_2 = 12$µm] for the second one, the amplification factor reaches respectively 0.22 and 1.2. These values are respectively 3 and 6 times higher than for the single-color pyrometry examples in previous paragraph.

The error on temperature can be lowered by reducing the equivalent wavelength, i.e. by increasing the distance between λ_2^{-1} and λ_1^{-1}, as for example by increasing the higher wavelength λ_2 or decreasing the shorter one λ_1. In any case the amplification factor will always be larger than the one obtained with single-color pyrometry performed at the shortest wavelength.

A common idea is that by choosing close wavelengths, there is a higher chance that the ratio $\varepsilon(\lambda_1)/\varepsilon(\lambda_2)$ gets near 1. However, in doing so, the equivalent wavelength λ_{12} increases and the sensitivity of the radiance ratio to temperature drops. A better strategy is to widen the spectral separation, more precisely to increase the λ_1^{-1}-λ_2^{-1} difference, (i.e. to decrease λ_{12}). Even for close wavelengths, the statement $\varepsilon(\lambda_1)/\varepsilon(\lambda_2)$=1 is prone to error. A prior knowledge of the ratio $\varepsilon(\lambda_1)/\varepsilon(\lambda_2)$ is thus required for evaluating T from eq. (5.18) or eq. (5.19). Having this in mind it is thus preferable maximizing the sensitivity to temperature as described before.

In single-color pyrometry at λ_1, the required prior knowledge is about $\varepsilon(\lambda_1)$. In two-color pyrometry it is about the ratio $\varepsilon(\lambda_1)/\varepsilon(\lambda_2)$. Obviously we can't avoid the introduction of some knowledge about the emissivity spectrum.

The advantage however as compared to one-color pyrometry is that thanks to the ratioing, the method is insensitive to problems like a partial occultation of the line of sight, or an optical path transmission variation (provided that this transmission variation is the same in both spectral channels).

For evaluating the emissivity ratio $\varepsilon(\lambda_1)/\varepsilon(\lambda_2)$ one could resort to pyroreflectometry [12]. Each emissivity is equal to $1 - \rho^{\cap}(\lambda,\theta,\varphi) = 1 - \pi\eta\rho''(\lambda,\theta_i,\varphi_i,\theta_r,\varphi_r)$ where η is a diffusion factor. It actually depends on incident and reflection directions as well as on wavelength. The bidirectional reflectance $\rho''(\lambda,\theta_i,\varphi_i,\theta_r,\varphi_r)$ is measured at the two wavelengths with the use of an additional source and a reference material in place of the tested one. It is then assumed that the diffusion factor is wavelength independent. This remaining unknown parameter is finally adjusted until the color temperatures at both wavelength (together

eventually with the ratio temperature) are made coincident. This common temperature is the true one.

In some circumstances, it is possible to bring close to the characterized object a highly reflecting surface. By properly choosing its shape, one gets two benefits: the reflection fluxes from the environment are diminished and the apparent emissivity of the sensed surface is increased thanks to the multiple reflections of the emitted radiation between the surface and the mirror [13]. As a consequence, the temperature estimation error due to errors on the emissivity ratio now refer to $\hat{\varepsilon}(\lambda_1)/\hat{\varepsilon}(\lambda_2)$ where $\hat{\varepsilon}$ is the apparent, actually amplified, emissivity. The errors are therefore diminished.

Instead of evaluating the temperature from the radiance ratio in eq. (5.18) or eq. (5.19), one could get it from a least squares minimization between the measured radiances S_1 at λ_1 and S_2 at λ_2 and their theoretical counterpart. The cost function expresses as:

$$J(T,\varepsilon(\lambda_1),\varepsilon(\lambda_2)) = [S_1 - \varepsilon(\lambda_1)B(\lambda_1,T)]^2 + [S_2 - \varepsilon(\lambda_2)B(\lambda_2,T)]^2 \qquad (5.22)$$

$$T = \min_{T,\varepsilon_1,\varepsilon_2} J(T,\varepsilon(\lambda_1),\varepsilon(\lambda_2)) \qquad (5.23)$$

This problem is underdetermined as there are three unknown parameters: T, $\varepsilon(\lambda_1)$ and $\varepsilon(\lambda_2)$ and only two observations: S_1 and S_2. One possibility for solving it is to introduce a functional relationship between the two emissivity values. An example of such relationship is:

$$\varepsilon(\lambda_1)/\varepsilon(\lambda_2) = \beta \qquad (5.24)$$

which correspond to the constant emissivity ratio already invoked in the course of the ratio method. In this context we actually have two methods for evaluating the temperature from the two spectral signals S_1 and S_2: either from their ratio in eq. (5.18) of from the least squares equation in eq. (5.22). The signals are actually corrupted by additive noise and it is known that the expected value of the ratio is a biased estimator of the ratio of the expected values. It is thus preferable using eq. (5.22) for the temperature identification.

Many other functional relationships could be used. Here are a few examples:

$$\varepsilon(\lambda_1) - \varepsilon(\lambda_2) = \beta \qquad (5.25)$$
$$1/\varepsilon(\lambda_1) - 1/\varepsilon(\lambda_2) = \beta \qquad (5.26)$$

where β is a surface dependent constant.

The emissivity compensation methods of Foley [14], Watari [15] and Anderson [16] described in [17] can all be connected to the following general relationship:

$$\varepsilon(\lambda_1) = \varepsilon(\lambda_2)^\beta \qquad (5.27)$$

where again β is a surface dependent constant (in [15] it is actually fixed to λ_1/λ_2).

The crucial point with two-color pyrometry is to find out a functional relationship like those in eq. (5.24) to eq. (5.27) together with the associated parameter β. It often happens that a good choice for a given material may lead to poor results for another material or for the same material in a different state (oxidation, ageing). The great difficulty, when dealing with different materials or with materials in different state, is to find out a general functional relationship able to represent all observed emissivity changes.

4. Multiwavelength Pyrometry

One can proceed further by adding measurements performed at other wavelengths. The problems still remains underdetermined, as one gets N radiance values, but in the same time one faces N+1 unknowns: N spectral emissivities and one temperature value.

Multiwavelength pyrometry has been a subject of controversy for several decades [11], [18]-[42]: some authors presented experimental results with various successes, sometimes with small temperature errors, other times with unacceptably high errors, depending on the material, on its surface state, and on the chosen function for approximating the emissivity spectrum. Even the theoretical works don't agree about the advantage of using a large number of wavelengths [18], [19], [23], [25], [27], [28], [29], [37], [38], [41], [42].

In the following we will present a few results which highlight the difficulty to obtain good and repeatable results with some multiwavelength approaches and a series of error mitigation processes.

4.1.   Interpolation based methods

For solving the underdetermined problem, a *potential* solution would be to reduce *simply by one* the degree of freedom of the emissivity spectrum. For this purpose a first approach consists in approximating $\varepsilon(\lambda)$ or $\ln[\varepsilon(\lambda)]$ by a polynomial of degree *N-2*:

$$\varepsilon_i \approx \sum_{j=0}^{N-2} a_j \lambda_i^{\ j} \qquad or \quad \ln(\varepsilon_i) \approx \sum_{j=0}^{N-2} a_j \lambda_i^{\ j} \qquad i=1,N \tag{5.28}$$

However, it was shown in [19], based on the Wien's approximation and a polynomial approximation of $\ln[\varepsilon(\lambda)]$ that this method can rapidly lead to unrealistic temperature values as *N* increases. Let us first assume that there is no measurement error ($S_i = L(\lambda_i,T)$). As a matter of fact, taking the logarithm of equation (5.17) with the Wien approximation for blackbody radiance, one gets:

$$\ln\left[S_i\,\lambda_i^{\,5}/C_1\right] = \ln\left[L(\lambda_i,T)\lambda_i^{\,5}/C_1\right] = \ln(\varepsilon_i) - C_2/\lambda_i T \qquad i=1,N \tag{5.29}$$

With the polynomial approximation of degree N-2 for $\ln[\varepsilon(\lambda)]$ in eq. (5.28), a temperature T' is retrieved instead of the real temperature T :

$$\ln\left[S_i\,\lambda_i^{\,5}/C_1\right] = \ln(\varepsilon_i) - C_2/\lambda_i T = \sum_{j=0}^{N-2} a_j \lambda_i^{\ j} - C_2/\lambda_i T' \qquad i=1,N \tag{5.30}$$

By multiplying eq. (5.30) by λ_i one can notice that T' is related to the constant parameter of the polynomial of degree *N*-1 interpolating the *N* values $\lambda_i \ln\left[S_i\,\lambda_i^{\,5}/C_1\right]$:

$$\lambda_i \ln\left[S_i\,\lambda_i^{\,5}/C_1\right] = \sum_{j=1}^{N-1} a_j \lambda_i^{\ j} - C_2/T' \qquad i=1,N \tag{5.31}$$

One can also notice that the temperature error expressed through $C_2\left(1/T - 1/T\,'\right)$ (it is also called "temperature correction") corresponds to the constant parameter of the polynomial of degree N-1 interpolating the N values $\lambda_i \ln[\varepsilon(\lambda_i)]$:

$$\lambda_i \ln(\varepsilon_i) = \sum_{j=1}^{N-1} a_j \lambda_i^{\,j} + C_2\left(\frac{1}{T} - \frac{1}{T'}\right) \qquad i = 1, N \tag{5.32}$$

The temperature corrections for N=1,2,3 are [11], [26]:

$$
\begin{aligned}
N = 1 \qquad & C_2\left(\frac{1}{T} - \frac{1}{T'}\right) = \lambda_1 \ln(\varepsilon_1) \\[2mm]
N = 2 \qquad & C_2\left(\frac{1}{T} - \frac{1}{T'}\right) = \frac{\lambda_1 \lambda_2}{\lambda_1 - \lambda_2} \ln\left(\frac{\varepsilon_2}{\varepsilon_1}\right) \\[2mm]
N = 3 \qquad & C_2\left(\frac{1}{T} - \frac{1}{T'}\right) = \frac{\lambda_1 \lambda_2 \lambda_3}{(\lambda_2 - \lambda_1)(\lambda_3 - \lambda_1)(\lambda_3 - \lambda_2)}\left(\lambda_1 \ln\left(\frac{\varepsilon_2}{\varepsilon_3}\right) + \lambda_2 \ln\left(\frac{\varepsilon_3}{\varepsilon_1}\right) + \lambda_3 \ln\left(\frac{\varepsilon_1}{\varepsilon_2}\right)\right)
\end{aligned}
\tag{5.33}
$$

The temperature correction involves the ratio $\varepsilon_1/\varepsilon_2$ for N=2. With equidistant wavelengths, it involves the ratio $\varepsilon_1\varepsilon_3/\varepsilon_2^{\,2}$ for N=3 and the ratio $\varepsilon_1\varepsilon_3^{\,2}/\varepsilon_2^{\,2}\varepsilon_4$ for N=4 [26]. These ratios are of course to estimate beforehand. Assigning arbitrarily a value of 1 to the emissivity ratio for a series of metals had the consequence that the temperature estimation error increased very rapidly with the number of wavelengths [26].

It can be shown that the temperature correction limit for wavelength intervals decreasing to 0 is equal to $(-1)^{N-1}\,\lambda^N/(N-1)!\,d^{N-1}\ln[\varepsilon(\lambda)]/d\,\lambda^{N-1}$ [23]. One can also recognize in eq. (5.32) that the temperature correction corresponds to the extrapolation at $\lambda=0$ of the polynomial interpolation of $\lambda_i \ln[\varepsilon(\lambda_i)]$ of degree N-1. This finding can now be developed a little more. If, *by chance*, a polynomial of degree N-2 could be found passing *exactly* through the N values $\ln[\varepsilon(\lambda_i)]$, the polynomial of degree N-1 passing through the N values $\lambda_i \ln[\varepsilon(\lambda_i)]$ would correspond to the previous one multiplied by λ; its constant parameter (i.e. the temperature correction term) would thus be equal to 0, and the retrieved temperature would be the exact one. The considered event is however highly improbable, therefore, in practice, there is an unavoidable bias. Furthermore the temperature error magnitude is tightly dependent on polynomial *extrapolation* properties. Unfortunately it is well known that an extrapolation based on a polynomial interpolation leads to increasingly high errors as the polynomial degree rises. Furthermore, things get progressively worse as the extrapolation is performed far from the interpolation domain. This last point would actually advocate expanding the spectral range to the shortest possible wavelength, but it is a desperate remedy.

The potentially catastrophic errors described just before are actually systematic errors, i.e. method errors. They are obtained even when assuming errorless spectral signals. For analyzing the influence of measurement errors, one can state, for simplicity, that the measurement error in channel i has the same impact as a corresponding uncertainty of the emissivity in the same channel, $d\varepsilon(\lambda_i)$. Then, the interpolation of the $\lambda_i \ln[\varepsilon(\lambda_i) + d\varepsilon(\lambda_i)]$ values leads to the same extrapolation errors as described before and finally adds to it. The calculated temperature is thus increasingly sensitive to measurement errors as the number of channels increases.

The poor success of the *interpolation based* method originates from the *over-fitting* of the experimental data. It was finally recognized that the *interpolation based* method could be considered only for the simpler pyrometers, i.e. with two or three wavelengths at most [19].

4.2.   Regularization by using a low-order emissivity model

4.2.1. Description of emissivity models

The over-fitting shortcomings previously described can be alleviated by reducing the number of unknown that are used for describing the emissivity spectrum. Different models were tested in the past:

$$\varepsilon(\lambda_i) = \sum_{j=0}^{m} a_j \lambda_i^{\,j} \quad i = 1,...,N \quad m < N-2 \text{ (generally } m=1 \text{ or 2)} \qquad (5.34)$$

$$\ln[\varepsilon(\lambda_i)] = \sum_{j=0}^{m} a_j \lambda_i^{\,j} \qquad i = 1,...,N \quad m < N-2 \text{ (generally } m =1 \text{ or 2)} \qquad (5.35)$$

$$\varepsilon(\lambda_i) = 1/(1 + a_0 \lambda_i^{\,2}) \qquad i = 1,...,N \qquad (5.36)$$

Polynomials of $\lambda^{1/2}$ or $\lambda^{-1/2}$ for $\ln[\varepsilon(\lambda)]$ and functions involving the brightness temperature were considered in [37], [38], a sinusoïdal function of λ in [18], and other more "physical" models like Maxwell, Hagen-Rubens and Edwards models in [11], [30], [41].

The grey-bands model consists in separating the spectrum in a small number of bands N_b and assigning the same emissivity value to all channels of a given band [25]. The bands can be narrowed down to three or even two channels as suggested in [76]. In this way, the number of unknowns is reduced from $N+1$ to $N/3+1$ or $N/2+1$. One can go even further by squeezing some bands to merely one channel. The extreme limit consists in $N-1$ single-channel bands plus one dual-channel band. In that case we face a problem with N measurements and N unknowns which is thus, *in principle*, invertible. We will see that it is actually very badly conditioned.

The concept of grey-bands can be generalized by allowing that the channels that are chosen to share a common emissivity value are not necessarily close together: an iterative process was described in [43] where these wavelengths are each time reshuffled according to the pseudo-continuous emissivity spectrum, i.e. the one defined over the *N* wavelengths according to:

$$\hat{\varepsilon}(\lambda_i, \hat{T}) = \frac{L(\lambda_i, T)}{B(\lambda_i, \hat{T})} \qquad i = 1,...,N \qquad (5.37)$$

where $\hat{T}$ is the most recent temperature estimation. $\hat{\varepsilon}(\lambda_i, \hat{T})$ is sorted from lower to higher values and the N_b bands of equal emissivity values are defined by splitting the $\hat{\varepsilon}(\lambda_i, \hat{T})$ vector in N_b parts.

The unknown parameters of the emissivity function, together with temperature, are finally evaluated through least squares minimization. By introducing the Wien approximation for radiance, a polynomial approximation for $\ln[\varepsilon(\lambda)]$ and by considering the observable $\ln\left[S_i \lambda_i^5/C_1\right]$, equation (5.30) shows that the problem reduces to a *linear least squares* problem in the coefficients a_j and in T^{-1} ([18], [22], [35], [36]). Otherwise, when considering for the observable the spectral signal S_i itself, one faces a *non-linear least squares* problem ([20], [21], [24], [25], [27]-[34], [36]-[42],[44]). Let us add that by rearranging the *i* equations as described in equation (5.30) one could get rid of one parameter, either a constant parameter or the temperature ([18][22][36]). However it is believed that no advantage in accuracy is expected by manipulating the data to present the same information in different form [18]. As a matter of fact, in the case of linear fitting such a manipulation even increases the uncertainty of the identified parameters.

We will now consider different aspects of the Least Squares Multiwavelength Pyrometry solution (LSMWP).

4.2.2. Least-squares solution of the linearized Emissivity Temperature Separation problem (ETS)

We will consider that the errorless signal corresponds to the emitted radiance expressed with the Wien's approximation. The chosen observable is actually the logarithm of the measured signal and we will admit that this observable is corrupted by an additive noise:

$$Y_i = \ln\left(S_i \lambda_i^5/C_1\right) = \ln\left(L_i \lambda_i^5/C_1\right) + e_i \qquad i = 1, N \qquad (5.38)$$

where e_i is the measurement error (noise) in channel *i*. We will assume that the e_i, *i=1,N* are uncorrelated random variables following a Gaussian distribution of uniform variance. It is usually assumed that the spectral signal, not its logarithm, is affected by a noise of uniform variance. For ease, we will consider here that it applies to its logarithm. This approximation is valid if the spectral range is not too wide with respect to the variations of the Planck's law $B(\lambda, T)$ and if the emissivity does not have too wide variations.

According to equation (5.30) where $\ln[\varepsilon(\lambda)]$ would be approximated by a polynomial of degree *m* only, the least squares solution is:

$$\hat{\mathbf{P}} = \begin{bmatrix} \hat{a}_0 & ... & \hat{a}_m & \hat{T} \end{bmatrix}^T = \arg\underset{a_j,T}{Min} \sum_{i=1}^{N}\left(Y_i - \left(\sum_{j=0}^{m} a_j \lambda_i^{j} - \frac{C_2}{\lambda_i T}\right)\right)^2 \qquad (5.39)$$

For numerical purposes, it is preferable to replace the wavelength in the polynomial expression by its reduced and centered value so that $\lambda_i* \in [-1,1]$:

$$\lambda_i* = 2\frac{\lambda_i - \lambda_{min}}{\lambda_{max} - \lambda_{min}} - 1 \qquad (5.40)$$

For the same reason, one can normalize T by T_{ref} so that $C_2/\lambda_i T_{ref}$ is of the order of 1. The associated unknown parameter is then $P_T* = T_{ref}/T$. The parameter vector is :
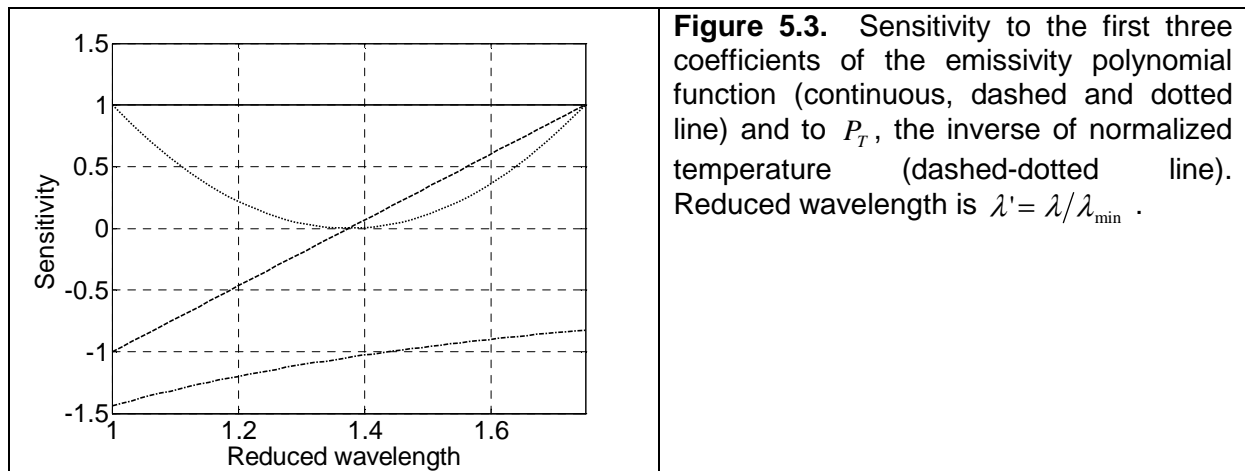
Lecture 5: Measurements without contact in heat transfer: page 13

$$\mathbf{P}* = \begin{bmatrix} a_0 * & ... & a_m * & P_T * \end{bmatrix}^T \qquad (5.41)$$

where the parameters $a_j *$ are the coefficients of the polynomial in $\lambda_i *$. The corresponding sensitivity matrix is:

$$\mathbf{X} = \begin{bmatrix} 1 & \lambda_1 * & \lambda_1 *^2 & ... & \dfrac{-C_2}{\lambda_1 T_{ref}} \\ ... & ... & ... & ... & ... \\ 1 & \lambda_N * & \lambda_N *^2 & ... & \dfrac{-C_2}{\lambda_N T_{ref}} \end{bmatrix}_{N,m+2} \qquad (5.42)$$

where the columns correspond to the sensitivity to successive parameters in vector $\mathbf{P} *$ (i.e. the first derivative of the model function relatively to each parameter).
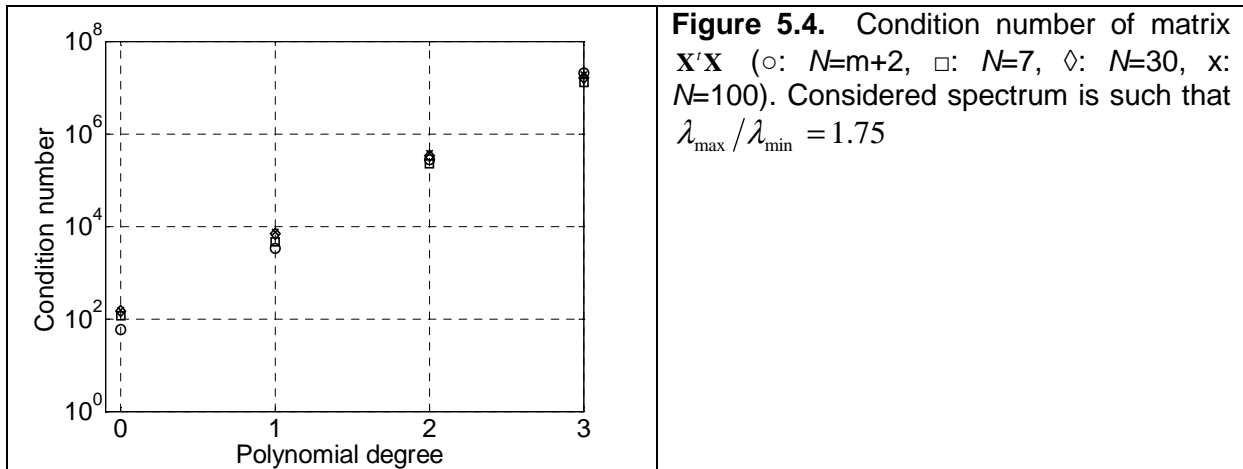
The sensitivity to the parameters $a_j *$ and to $P_T *$ is plotted vs. the reduced wavelength $\lambda_i ' = \lambda_i / \lambda_{min}$ in figure 5.3 up to j=2 for the particular case of $\lambda_{max} / \lambda_{min} = 1.75$. The sensitivity to the temperature inverse is very smooth, close to linear. We thus expect a strong correlation between the parameters (near collinear sensitivity vectors).

Figure 5.3. Sensitivity to the first three coefficients of the emissivity polynomial function (continuous, dashed and dotted line) and to P_T, the inverse of normalized temperature (dashed-dotted line). Reduced wavelength is $\lambda' = \lambda / \lambda_{min}$.

An estimation of the parameter vector $\mathbf{P} *$ in the least squares sense is obtained by solving the linear system:

$$\left(\mathbf{X}^T \mathbf{X} \right) \hat{\mathbf{P}}* = \mathbf{X}^T \mathbf{Y} \qquad (5.43)$$

The near-dependent sensitivities lead to a $\mathbf{X}^T \mathbf{X}$ matrix that is near-singular. Indeed by computing the condition number of the matrix $\mathbf{X}^T \mathbf{X}$ one gets very high values, even for a low degree polynomial approximation (see figure 5.4).

Figure 5.4. Condition number of matrix $\mathbf{X}'\mathbf{X}$ (○: N=m+2, □: N=7, ◊: N=30, x: N=100). Considered spectrum is such that $\lambda_{max}/\lambda_{min} = 1.75$

The condition number describes somehow the rate at which the identified parameters will change with respect to a change in the observable. Thus, if the condition number is large, even a small error in the observable may cause a large error in the parameters (the condition number however only provides an upper bound). The condition number also reflects how a small change in the matrix $\mathbf{X}^T\mathbf{X}$ itself will affect the identified parameters. Such a change may be due to the measurement error of the equivalent wavelength corresponding to each spectral channel. From figure 5.4, a first statement is that the regularization with a polynomial model of degree 2 or higher will not be efficient. But even the case of a polynomial of degree 1 is expected to show unstable results.

The condition number is not all. By the way, it depends on the choice of the reference temperature T_{ref}. Sometimes it could even be misleading because it only gives an upper bound of the error propagation. It is better to analyze the diagonal values of the covariance matrix $(\mathbf{X}^T\mathbf{X})^{-1}$. They actually provide the variance amplification factor for each identified parameter $P*$:

$$\left[\sigma_{P*}^{2}\right] = diag\left((\mathbf{X}^T\mathbf{X})^{-1}\right)\sigma^2 \tag{5.44}$$

where σ^2 is the variance of the observable, i.e. $(\sigma_{S_i}/S_i)^2$ which is here assumed independent of the spectral channel i (if instead one assumes that the radiance variance $(\sigma_{S_i})^2$ is uniform, the result would be $\left[\sigma_{P*}^{2}\right] = diag\left((\mathbf{X}^T\mathbf{\Psi}^{-1}\mathbf{X})^{-1}\right)$ where $\mathbf{\Psi}$ is the inferred covariance matrix of the observable).

One should be aware that σ_{P*}^{2} merely describes the error around the mean estimator value due to the radiance error propagation to the parameters. If the mean estimator is biased, as it is the case when the true emissivity profile is not well represented by the chosen model, one should add the square *systematic error* to get the RMS error which better represents the misfit to the true parameter value, either the temperature or a spectral emissivity value (this will be described later through a Monte-Carlo analysis of the inversion).

With the polynomial model, the mean standard relative error for emissivity, which is defined by:

$$\frac{\sigma_\varepsilon}{\varepsilon} \equiv \sqrt{\frac{1}{N}\sum_{i=1}^{N}\frac{\sigma_{\varepsilon_i}^{\,2}}{\varepsilon_i^{\,2}}} \tag{5.45}$$

is related to the standard error of the retrieved polynomial coefficients through:

$$\frac{\sigma_\varepsilon}{\varepsilon} = \sqrt{\frac{1}{N}\sum_{i=1}^{N}\left[X_{ij}^{\,2}\right]^T\left[\sigma_{a_{j*}}^{\,2}\right]_{j=1,m}} \tag{5.46}$$

As such, it can be related to the uncertainty of the observable, which will be written σ_S/S, through an error amplification factor K_ε:

$$\frac{\sigma_\varepsilon}{\varepsilon} = K_\varepsilon \frac{\sigma_S}{S} \tag{5.47}$$

With the grey-bands model, the mean standard error and the amplification factor are defined according to:

$$\frac{\sigma_\varepsilon}{\varepsilon} \equiv \sqrt{\frac{1}{N}\sum_{i=1}^{N_b}\left(\frac{\sigma_{\varepsilon_i}}{\varepsilon_i}\right)^2} = K_\varepsilon \frac{\sigma_S}{S} \tag{5.48}$$

From the Wien expression for radiance, it is clear that the standard relative error for temperature is proportional to temperature, to σ_S/S, and to a wavelength scale representative of the spectral window $\tilde{\lambda}$ (one can choose the geometric mean of the window limits: $\tilde{\lambda} \equiv \sqrt{\lambda_{min}\lambda_{max}}$). The error amplification factor for temperature, K_T, is thus defined according to:

$$\frac{\sigma_T}{T} = K_T \tilde{\lambda} T \frac{\sigma_S}{S} \tag{5.49}$$

The error amplification factors K_T and K_ε are plotted in figure 5.5 for the polynomial model, assuming a relative bandwidth $\lambda_{max}/\lambda_{min}$ of 1.75 (this could correspond to the [8µm-14µm] spectral interval, for example).
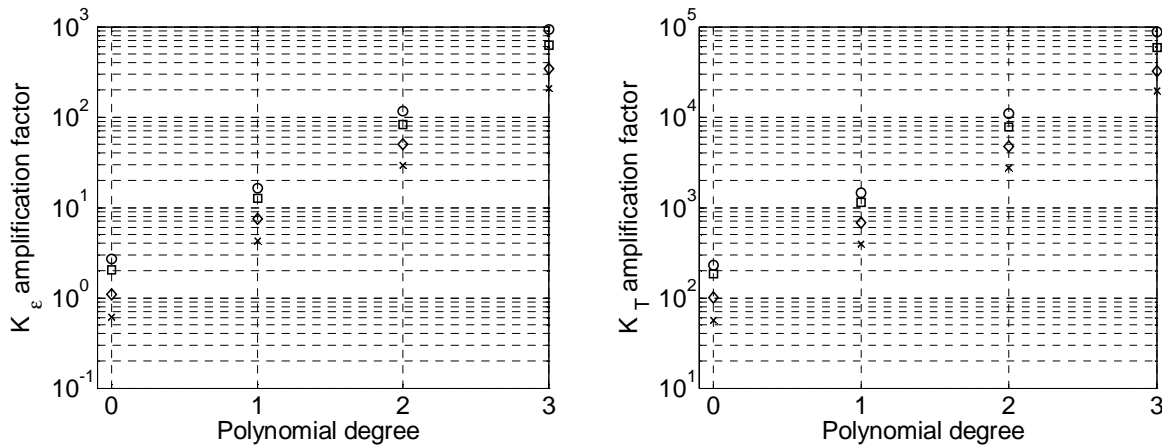
Figure 5.5. Left : Error amplification factor of emissivity versus the polynomial degree m chosen for modeling $\ln[\varepsilon(\lambda)]$. Symbols correspond to different values for the total number of spectral channels: ○: $N=m+2$, □: $N=7$, ◊: $N=30$, x: $N=100$. Right : Same for the error amplification factor of temperature

A first comment about the polynomial model is that the standard errors increase exponentially with the polynomial degree m, roughly like $\exp(2m)$. This increase can be slowed down by widening the spectral window. With the grey-bands model, the standard errors increase nearly in proportion to the number of bands. In both cases, they decrease with the total number of channels, roughly like $N^{-1/2}$. Empirical relations can be found for the factors K_T and K_ε. They lead to the following error predictions for the polynomial model, in the particular case $\lambda_{max}/\lambda_{min}$ = 1.75:

$$\begin{cases} \dfrac{\sigma_T}{T} \cong 420 \dfrac{\exp(1.94m)}{\sqrt{N+4}} \tilde{\lambda} T \dfrac{\sigma_S}{S} \\ \dfrac{\sigma_\varepsilon}{\varepsilon} \cong 6.4 \dfrac{\exp(1.93m)}{\sqrt{N+4}} \dfrac{\sigma_S}{S} \end{cases}$$

(5.50)

Regarding the bandwidth influence, let us notice that the relative error of temperature depends both on λ_{min} and λ_{max} whereas the mean relative error of emissivity only depends on the ratio $\lambda_{max}/\lambda_{min}$.

Assuming a target at 320K, and 1% radiance noise, a pyrometer with seven wavelengths between 8μm and 14μm will provide temperature and emissivity values with standard errors as reported in Table 5.1, depending on the polynomial degree chosen for $\ln[\varepsilon(\lambda)]$.

Table 5.1. Root-mean square error for the estimated temperature and emissivity depending on the degree of the polynomial model for emissivity. Target temperature is 320K and radiance noise is 1%.

Polynomial degree	σ_T (K)	σ_ε
0	1.5	0.02

1	9.4	0.13
2	64	0.83

The errors are rather high with a linear model for $\ln[\varepsilon(\lambda)]$ and they reach unacceptably high values when using a degree 2 polynomial. These results seem to preclude using the least squares linear regression approach together with a polynomial of degree 2 and more. They were obtained with the Wien's approximation. However, Planck's law is close to the Wien's approximation over a large spectrum, therefore we expect that the general least squares nonlinear regression based on the Planck's law will also face serious problems when using a polynomial model for emissivity.

Let us recall that the temperature and emissivity errors mentioned here only describe how the radiance error propagates to the parameters. It was here assumed that the emissivity spectrum *perfectly* matches the considered polynomial model. If it is not the case (which actually occurs almost every time) a *systematic error* appears and the joint errors will be presented in § 4.2.4 through a Monte-Carlo analysis.

Applying the grey-bands model to the previous example leads to the standard errors shown in Table 5.2 (the number of bands can be increased up to *N*-1=6 while avoiding underdetermination).

Table 5.2. Root-mean square error for the estimated temperature and emissivity depending on the number of bands when assuming a grey-band model for emissivity and 7 spectral measurements. Target temperature is 320K and radiance noise is 1%.

Number of bands	σ_T (K)	σ_ε
1	1.5	0.020
2	2.6	0.035
3	3.7	0.049
4	5.7	0.076
5	6.7	0.090
6	7.2	0.094

The errors increase with the number of bands, starting from the values corresponding to a degree 0 polynomial and ending at values that are lower than those obtained with a degree 1 polynomial. This is interesting in the sense that even with six bands, i.e. six degrees of freedom for emissivity, the errors don't "explode" as it was observed before by increasing the polynomial degree. The grey-bands model, although not being smooth, could thus capture more easily rapid variations in the emissivity profile like peaks.

However, as stated before, the standard errors that are here presented only reflect what happens when noise corrupts the radiance emitted by a surface which otherwise *perfectly follows the staircase model*. As an example, with the 6-bands case, the emissivity should be *equal* in the two channels that were chosen to form the largest band.
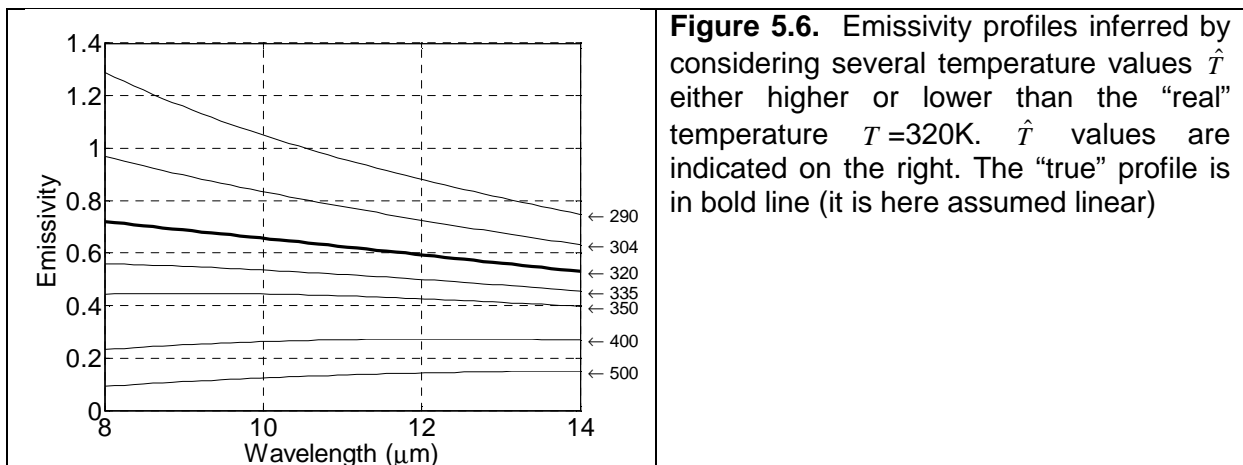
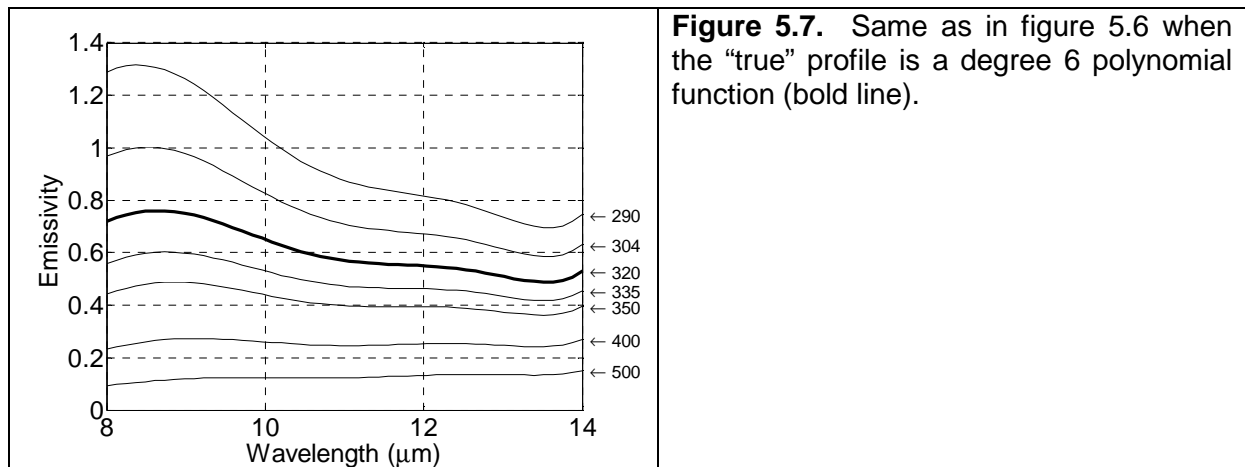### 4.2.3. A look on the solutions of the ETS problem

Another way of presenting the ill-posedness of the ETS problem and the difficulties in finding an appropriate regularization consists, like in [19], in exposing the multiple solutions to this underdetermined problem. For this purpose we took two examples for the "true" emissivity profile: either a linear profile or a polynomial of degree 6. These profiles are represented with bold lines in figure 5.6 and in figure 5.7.
The emitted radiance was then calculated according to Planck's law assuming a temperature $T = 320$K in both cases (for simplicity we discarded at this stage the eventual reflections; experimental noise was also discarded, it will be added later). Then, from different temperature estimated values $\hat{T}$, one can infer the emissivity profile $\hat{\varepsilon}(\lambda,\hat{T})$ which *exactly* leads to the observed radiance. The estimated emissivity profile is given by:

$$\hat{\varepsilon}(\lambda,\hat{T}) = \frac{L(\lambda,T)}{B(\lambda,\hat{T})} = \varepsilon(\lambda)\frac{B(\lambda,T)}{B(\lambda,\hat{T})} \tag{5.51}$$

Some profiles $\hat{\varepsilon}(\lambda,\hat{T})$ are reported in figures 5.6 and 5.7 together with the corresponding initially estimated temperature values $\hat{T}$. We must stress the point that these emissivity profiles together with the corresponding $\hat{T}$ value are all *perfect solutions* to the problem, at least from the mathematical perspective. As a matter of fact they all lead to the observed radiance. Of course one has to discard the emissivity profiles presenting values higher than 1. With this constraint in mind, the admissible temperatures are from about 304K up. Similarly, profiles that reach values less than, say, 0.02-0.03 can also be discarded if one has some prior information that the surface is not a very clean polished metal surface.

Figure 5.6. Emissivity profiles inferred by considering several temperature values $\hat{T}$ either higher or lower than the "real" temperature T =320K. $\hat{T}$ values are indicated on the right. The "true" profile is in bold line (it is here assumed linear)

Figure 5.7. Same as in figure 5.6 when the "true" profile is a degree 6 polynomial function (bold line).

The traditional way consists in looking for a solution of $\varepsilon(\lambda)$ in the form of a polynomial and performing a least squares regression on the emitted radiance. As an example let us consider the case of a polynomial of degree 1. The problem can then be reformulated like this: it consists in finding in figure 5.6, respectively in figure 5.7, *the profile which is closest to a straight line*. The closeness criterion should take into account a weighting by the blackbody radiance function having in mind the least squares regression on the emitted radiance. Of course, in figure 5.6, the profile corresponding to $\hat{T}$ =320K is the only one to be linear (the curvature of the profile changes on each side of $\hat{T}$ =320K). If there is no error on the measured radiance, the perfect match is then for $\hat{T}$ =320K. Nevertheless, one has to admit that the profiles corresponding to an estimated temperature in the range 304K< $\hat{T}$ <350K are not far from a straight line. If one added some experimental noise, it is clear that the squared residuals after the linear fit would be in the same range for all profiles $\hat{\varepsilon}(\lambda,\hat{T})$ corresponding to this temperature range.

The case in figure 5.7 is even worse: it is evident that, among all possible solutions, the "true" profile is not the closest one to a straight line. Evidently, in this example, the answer for optimal $\hat{T}$ will be a temperature much higher than the "true" value (lower profiles in the figure are indeed smoother than higher profiles). The final solution will thus present a bias. A bias would also be obtained for the case drawn in figure 5.7 if the chosen emissivity model was a degree 0 polynomial instead of a degree 1 polynomial.

As often stated, when using LSMWP, it is necessary to choose an emissivity model that *exactly* corresponds to the true profile. The difficulty is that most often, the profile shape is unknown. A misleading thought is that LSMWP performs a fit of the true profile with the chosen model (polynomial, exponential, and so on). Actually, as seen above, performing LSMWP comes to choosing among the different possible profile solutions $\hat{\varepsilon}(\lambda,\hat{T})$, the one which fits at best to the model, in the least squares sense by weighting it with the blackbody radiance (the fit deals with $\varepsilon(\lambda)$ if the observable is radiance and with $\ln(\varepsilon(\lambda))$ if it is the logarithm of radiance). This can lead to an emissivity profile of much higher or much lower mean value than the real one, together with an important temperature error. Actually, the problem with present LSMWP is that it sticks to the emissivity *shape* rather than to its *magnitude*.

4.2.4. Least squares solution of the non linearized ETS problem

When using the Planck's law instead of the Wien's approximation, LSMWP cannot be linearized anymore. The nonlinear least squares problem can be tackled with the Levenberg-Marquardt method as provided for example by the *lsqnonlin* function from MATLAB library. When choosing a linear model for emissivity and when the "true" emissivity profile is indeed linear this naturally leads to the right temperature and the right emissivity profile (there is no systematic error when the simulated emissivity spectrum corresponds to the chosen model). On the contrary, when the "true" emissivity profile is not linear, the identification presents a bias. For a "true" emissivity profile corresponding to the bold line curve in figure 5.7, the result is reported in figures 5.8 and 5.9. For this example we assumed seven equidistant spectral measurements between 8 µm and 14 µm. The dots in figure 5.8 correspond to the simulated measured radiance (no noise at this stage) and the line corresponds to the radiance calculated from $\hat{L}(\lambda,T) = \hat{\varepsilon}_{d1}(\lambda)B(\lambda,\hat{T})$ where $\hat{\varepsilon}_{d1}(\lambda)$ is the degree 1 polynomial solution of the LSMWP inversion. A perfect match for radiance is of course impossible: the low order model chosen for emissivity (degree 1 polynomial) cannot explain the observed radiance variations. The least squares procedure reveals that the $\hat{\varepsilon}(\lambda,\hat{T})$ profile in figure 5.7 that fits at best to a straight line (taking into account the weighting with the blackbody radiance), is the one corresponding to a temperature of 335.3K. The seven dots in figure 5.9 correspond to $\hat{\varepsilon}(\lambda,335.3)$ and the dotted line is the best linear estimate for emissivity $\hat{\varepsilon}_{d1}(\lambda)$. The systematic error is thus +15K for temperature and between -0.06 and -0.2 for emissivity.
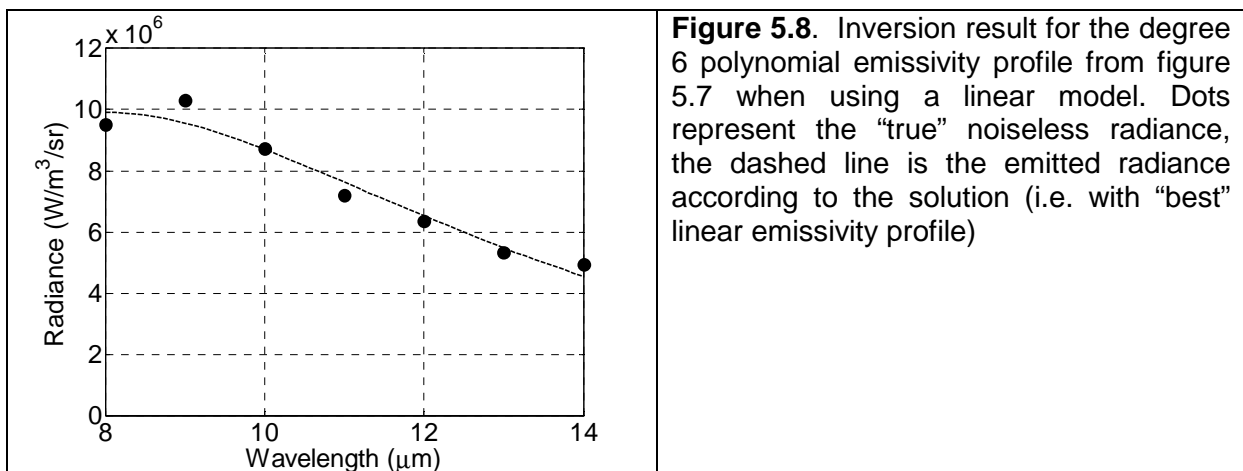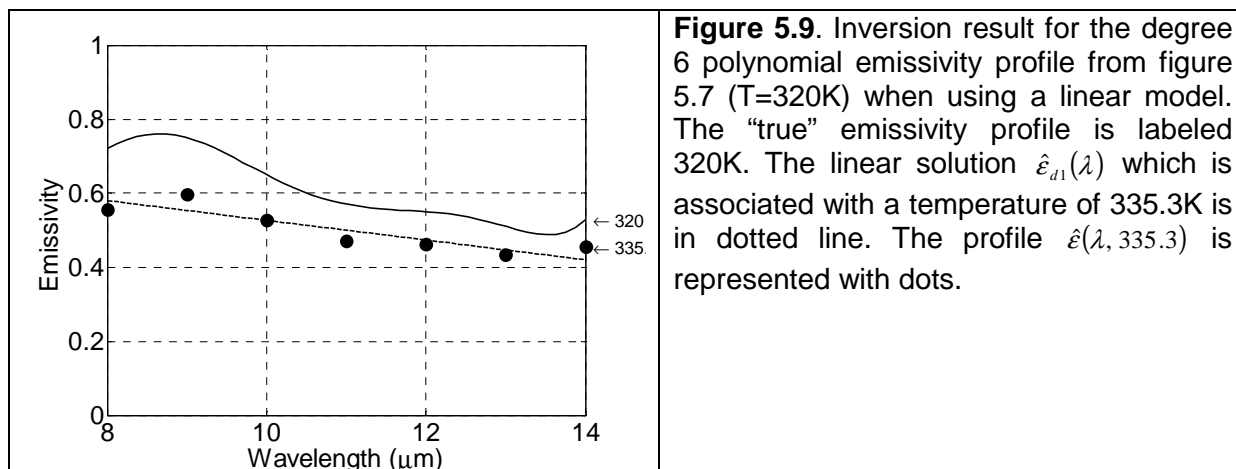

Figure 5.8. Inversion result for the degree 6 polynomial emissivity profile from figure 5.7 when using a linear model. Dots represent the "true" noiseless radiance, the dashed line is the emitted radiance according to the solution (i.e. with "best" linear emissivity profile)

Figure 5.9. Inversion result for the degree 6 polynomial emissivity profile from figure 5.7 (T=320K) when using a linear model. The "true" emissivity profile is labeled 320K. The linear solution $\hat{\varepsilon}_{d1}(\lambda)$ which is associated with a temperature of 335.3K is in dotted line. The profile $\hat{\varepsilon}(\lambda, 335.3)$ is represented with dots.

If the fitting happened be too far from the $\hat{\varepsilon}(\lambda, \hat{T})$ profile, one should change the model. For this particular example, however, changing to a quadratic model leads to a complete failure: the profile in figure 5.7 that is closest to a degree 2 polynomial is the one corresponding to 230K and the retrieved (hypothetical) emissivity spectrum ranges between 2 and 6 ! Obviously one should impose the constraint $\hat{\varepsilon}(\lambda, \hat{T})$ <1. The acceptable solution would then be the profile associated to $\hat{T}$ =304K which nethertheless means a 16K underestimation.

Let us now analyze the influence of the measurement noise on the temperature and emissivity separation performance. This can be easily performed by simulating experiments where the theoretical radiance is corrupted with artificial noise. The radiance is altered by adding values that are randomly generated with a predetermined probability density function. We assumed a Gaussian distribution with a spectrally uniform standard deviation. We fixed it to a value ranging from 0.2% to 6% of the maximum radiance (additive noise). The least squares minimization was performed without constraint (i.e. without imposing ε_i <1) in order to highlight the mathematical (poor) stability of the inversion procedure. A series of 200 radiance spectra were treated for each noise level and for both nominal emissivity profiles described in figures 3.6 and 3.7 (polynomial functions of degree 1 or 6). As before we assumed that the spectral measurements are performed at seven equidistant wavelengths between 8 µm and 14 µm. We chose a linear emissivity model for the LSMWP inversion. The results for the maximum root mean square emissivity error among the seven channels are plotted in figure 5.10-left. Those for the root mean square error on temperature are plotted in figure 5.10-right. One can notice that:

- when the "true" profile is linear (crosses), the RMS error on temperature and on emissivity increases proportionally to the radiance noise level (the temperature RMS error becomes somewhat erratic when noise is higher than about 3%). In particular, the RMS errors are 0.1 for emissivity and 8K for temperature in the case of a 1% measurement noise.
- when the "true" profile is a degree 6 polynomial (circles), the RMS errors are first dominated by the systematic error, which corresponds to the model implementation error (the chosen model – degree 1 polynomial – is too crude for representing the "true" profile); statistic errors due to the measurement noise dominate only when

noise is higher than 2-3%. The RMS errors are 0.2 for emissivity and 17K for temperature in the case of a 1% measurement noise.
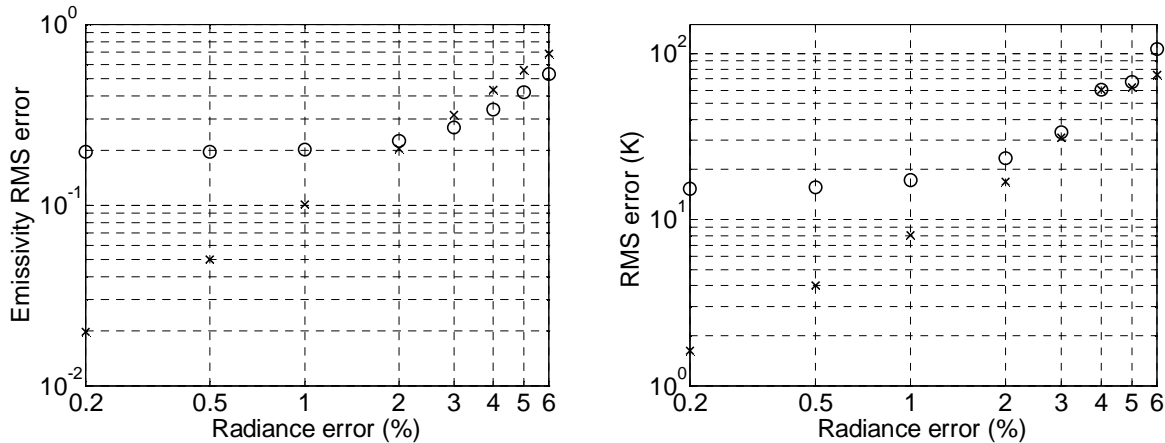

Figure 5.10. Statistic analysis (Monte Carlo sampling with 200 simulated experiments) of the measurement noise influence on the identified emissivity when using a linear emissivity model. The "true" emissivity was considered linear (crosses) or a degree 6 polynomial (circles). Multispectral measurement in seven channels between 8 and 14µm. Left : emissivity error, Right : temperature error.

Let us also add that the inversion leads to a systematic error as soon as the "true" profile departs from a straight line. The previous analysis allows us to evaluate the magnitude of this error when the deviation is small. Statistically, by considering several "true" profiles close to the nominal straight line in figure 5.6, the RMS of the systematic errors would be equal to the RMS of the statistic errors obtained by adding the same amount of measurement noise. For this reason, a "true" profile departing by as little as 1% from a straight line leads to an emissivity bias whose RMS value is about 0.1. The temperature quadratic mean error is in this case about 8K which is far from negligible. This result highlights the considerable importance of choosing the right emissivity model. This impact can be reduced by increasing the number of spectral channels (the trend is like $N^{-1/2}$ as seen later), at the condition that the departure from the profile model is randomly distributed.

The same analysis was performed by assuming that both the "true" profile and the model are quadratic. The RMS errors (not presented here) are roughly proportional to the radiance noise level like when both profiles are linear however at a much higher level: in the case of a 1% measurement noise, the RMS errors reach 0.33 for emissivity and 49K for temperature.

It is well known that statistic errors can be reduced by increasing the number of measurements, here by increasing the number of channels. This is confirmed in figure 5.11 where this number was increased from 7 to 120, keeping the channels uniformly distributed between 8µm and 14 µm. For this illustration the radiance measurement noise was fixed at 1%. One can notice that the RMS errors indeed decrease in the case of the linear "true" profile with a power-law trend, close to the $N^{-1/2}$ classical reduction. In the case of the more complicated degree 6 polynomial "true" profile there is no such reduction. As a matter of fact, systematic errors always dominate. There is even a progressive increase of the RMS errors

with the number of wavelengths. The RMS errors of 0.2 for emissivity and 17K for temperature that are observed with 7 channels cannot be reduced by adding more channels.
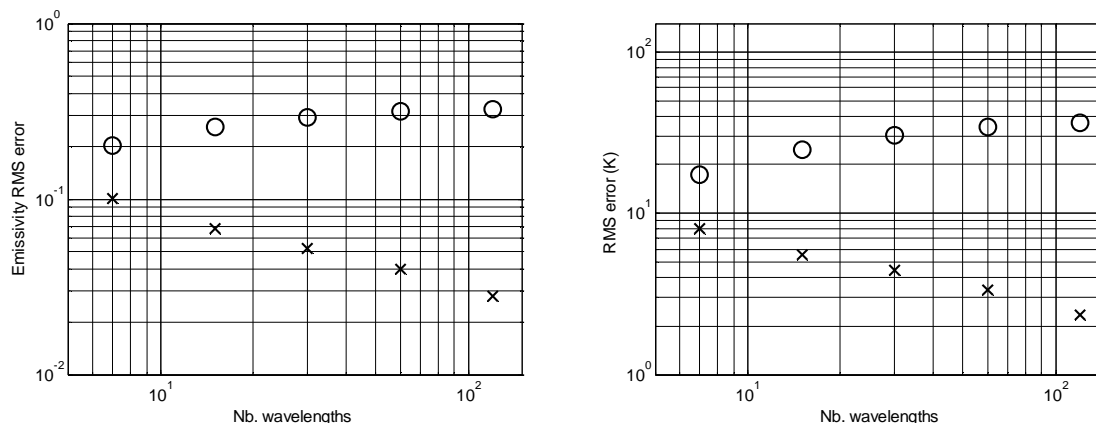

Figure 5.11. Same as in figure 5.10 when keeping a 1% gaussian noise for radiance but progressively increasing the number of channels from 7 to 120 (uniformly distributed between 8µm and 14µm).

As a conclusion we can state that:

- Even by reducing the number of unknowns, as was done here by modeling spectral emissivity with a polynomial of low degree, the problem remains badly conditioned; with a polynomial model (either for $\varepsilon(\lambda)$ or for $\ln\varepsilon(\lambda)$), reasonable inversion results are expected only up to degree 1.
- Important systematic errors appear as soon as the real emissivity departs from the considered model: 1% departure from a straight line already leads to 8K RMS error. More complicated spectral shapes lead to unpredictably high systematic errors (17K for the considered example of a degree 6 polynomial).
- Even if the real emissivity values at the sampled wavelengths ε_i i=1,N perfectly fitted to a straight line, the demand on radiance measurement precision is very high: as a matter of fact no more than 0.12% noise is allowed to get a 1K RMS error near room temperature for a 7-band pyrometer between 8µm and 14µm.

The same analysis was performed by considering the grey-bands model [2]. One noticed that for some particular number of bands, the results are significantly better than with the linear emissivity model. However, the results may vary by a factor of two by just changing by one the number of bands. This unpredictable behavior seems to preclude the grey-bands model from leading to a safer and more efficient inversion than with the linear emissivity model.

Finally, LSMWP is not performing well for simultaneous evaluation of temperature and emissivity when using the emitted spectral radiance only. Reasonable RMS values can be obtained only when the emissivity spectrum perfectly matches with the implemented emissivity model (grey-bands or linear). Otherwise, important systematic errors are encountered. The problem is that, apart from a few exceptions, one does not know beforehand whether the emissivity of a tested material complies with such or another model.

As a conclusion, it would seem that there is no valuable reason for implementing LSMWP in place of the simpler one-color or bispectral pyrometry. All methods need an a-priori information about emissivity. However the requirements with one-color pyrometry (the knowledge of an emissivity level) or with bispectral pyrometry (the knowledge of the ratio of emissivity at two wavelengths) are less difficult to satisfy than the requirement with LSMWP which is *a requirement of a strict shape conformity* of the emissivity profile with a given parametric function which, practically, is impossible to satisfy.

Regarding LSMWP, one must finally admit that without a knowledge about the emissivity *magnitude*, the temperature measurement cannot be very precise. Some vague intuition about the shape of the emissivity spectrum is not sufficient and adding more wavelengths doesn't help much. The blackbody spectrum is too regular, therefore, introducing an emissivity polynomial model of higher degree than 1 introduces high correlations and generally leads to poor results.

4.3.   Another multiwavelengh approach: the TES method

The TES method is a multiwavelength approach that was developed for land-surface temperature evaluation through infrared remote sensing, more specifically for the Advanced Space-borne Thermal Emission and Reflection Radiometer (ASTER) on board TERRA satellite [45]. It is a five-channel multispectral thermal–IR scanner.

TES is based on the observation that the relative spectrum $\beta(\lambda) = \hat{\varepsilon}(\lambda)/\bar{\hat{\varepsilon}}$ where the apparent emissivity $\hat{\varepsilon}(\lambda)$ is obtained from an estimation of temperature $\hat{T}$ according to:

$$\hat{\varepsilon}\left(\lambda,\hat{T}\right) = \frac{L(\lambda,T) - L^{\downarrow}(\lambda)}{B\left(\lambda,\hat{T}\right) - L^{\downarrow}(\lambda)} \tag{5.52}$$

is relatively insensitive to the temperature estimation error. A crude estimation as with the Normalized Emissivity Method (NEM) is thus sufficient [45]. The question is then how extracting the absolute spectrum $\hat{\varepsilon}(\lambda)$ from the relative spectrum $\beta(\lambda)$. Gillespie et al. [45] found out a correlation between ε_{min} and the minimum-maximum emissivity difference defined by $MMD = \beta_{max} - \beta_{min}$:

$$\varepsilon_{min} \approx 0.994 - 0.687\,MMD^{0.737} \tag{5.53}$$

The regression was based on 86 laboratory reflectance spectra from the ASTER spectral library [6] for soils, rocks, vegetation, snow, and water between 10 and 14µm. Ninety five percent of the samples fall within 0.02 emissivity units of the regression line. Nevertheless, this empirical relation in not universal: data related to artificial materials like metals fall far below the regression line.

After evaluating ε_{min} from the regression law, one retrieves a new estimate of the emissivity spectrum through

$$\hat{\varepsilon}(\lambda) = \beta(\lambda)\frac{\varepsilon_{min}}{\beta_{min}} \tag{5.54}$$

The temperature $\hat{T}$ is finally obtained by inverting the Planck's law in eq. (5.52) where λ is at the maximum emissivity value $\hat{\varepsilon}(\lambda)$. One or two iterations are sufficient for the convergence of the procedure.

To be effective, TES requires at least three or four spectral bands. TES doesn't work well for near-grey materials (as a matter of fact $\varepsilon_{\min}$ would then stick to the 0.994 value).

TES algorithm is presently used to calculate surface temperature and emissivity standard products for ASTER, which are predicted to be within respectively +1.5K and 0.015 of correct values. Validations performed on different sites demonstrated that TES generally performs within these limits.

The regression law:

$$\varepsilon_{\min} \approx 0.999 - 0.777\, MMD^{0.815} \tag{5.55}$$

was obtained using 108 emissivity spectra from the ASTER library, without man-made materials. It was compared with spectra of manmade materials used over urban surfaces in [47] (see fig. 5.11). The correlation in eq. (5.55) is relatively good for most considered manmade materials. Metallic surfaces are however badly modeled by this empirical relationship.
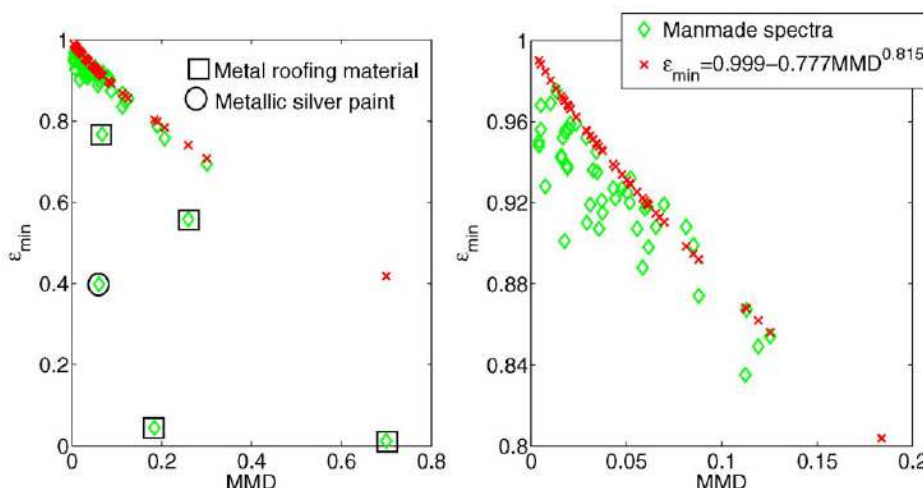

Figure 5.11. Correlation between MMD and $\varepsilon_{\min}$ in eq. (5.54) and comparison with 54 man-made materials spectra. Right figure is a detail from left plot [47].

The RMSE for emissivity is 0.017 in average (for a series of 9 manmade urban materials excluding metallic materials: brick, glass, tile, asphalt, concrete, marble, cement) and it may rise to 0.03 for some materials like marble and glass. Simultaneously, the RMSE for temperature is 0.9K in average and may rise to 1.5-1.8K for marble and glass ('true' temperature was set between 295K and 310K) [47].

The TES method is performing well for natural materials and man-made materials (excluding metallic materials) in the context of remote sensing. This concept could be extended to other situations. The decisive point would be to find out an empirical relation of the type in eq. (5.53) or (5.55) from the spectra of the considered materials.

5. Infrared systems calibration

Prior to any measurement using an infrared device, it is important to be aware of the limitations of the technique, but also of the transfer function of the device. Some work,

concerning either the thermography technique [48, 49] or the associated metrology [50-53] are available in the literature.

There are three major points of necessary characterization of the devices: inaccuracies of the calibration, spatial non-uniformity, and irregular time sampling can lead to false parameter estimation.

5.1.   Thermal calibration

In order to obtain reliable results, the user must, first of all, be confident in the apparatus calibration. Most of the time, infrared devices have their own setting and acquisition applications, including data-processing applications for digitizing, non-uniformity corrections, display, basic operations…

Generally, the calibration laws used by manufacturers suppose the sensor's response is linear, and consider the differences between the pixels' responses only as distributions of gains and offsets. The calibration of the device consists then in two distinct operations: the calibration of the average of a central area, and the application of maps of gains and offsets to link the response of each pixel to the one of the average of the sensor matrix. This second operation is called "Non-Uniformity Correction" (NUC).

In most cases, the calibration law is taken in the form of a 2 or 3 degree polynomial, more rarely a Planck-type law.

$$L_m(T) = aT^2 + bT + c \qquad (5.56)$$

$$L_m(T) = \frac{R}{\left[\exp\left(\dfrac{B}{T}\right) - F\right]} + Offset \qquad (5.57)$$

Where (a, b, c) or (R, B, F and offset) are parameters identified during the calibration, and Lm the radiance measured by the camera, expressed in arbitrary units.

The gains and offsets maps are computed so as to obtain uniform distributions of digitized fluxes for two specific images of uniform thermal scenes taken at two different temperatures; these two scenes are generally obtained by means of an extended blackbody. Recently, some manufacturers proposed to go further, by linking the values of the gain and offset maps an "internal temperature" of the camera, in order to compensate the thermal drifts associated with the heat produced by the internal electronics and the heat exchanges between the camera and its environment. This "advanced" non-uniformity correction is often called "Compensated Non-Uniformity Correction": CNUC.

Moreover, sensor matrixes always include some defective pixels (generally less than 0.5%), that can be saturated pixels, noisy pixels, or even "dead" pixels. They are localized using criteria dealing mainly with the discrepancy with respect to the mean response (in terms of digitized flux, gain, offset, etc.). Manufacturers propose to replace the value of these pixels by the one of their nearest non-defective neighbour (Bad Pixel Replacement, or BPR procedure), that induce a complete local correlation.

The validity of the standard calibrations can be easily checked out by observing a given thermal scene with a unique camera, but using different calibrations, associated with different

acquisition settings (integration time / measurement range). As an illustration, figure 5-2 illustrates different observations on a blackbody using different infrared cameras. These two illustrations show that it is appropriate, if possible, to use the centre of the matrix and the middle of the calibration range when using the manufacturer's calibration laws. If the application needs a wider measurement area, it could be convenient to take into account the dispersion of the measured values in the data treatment procedure.
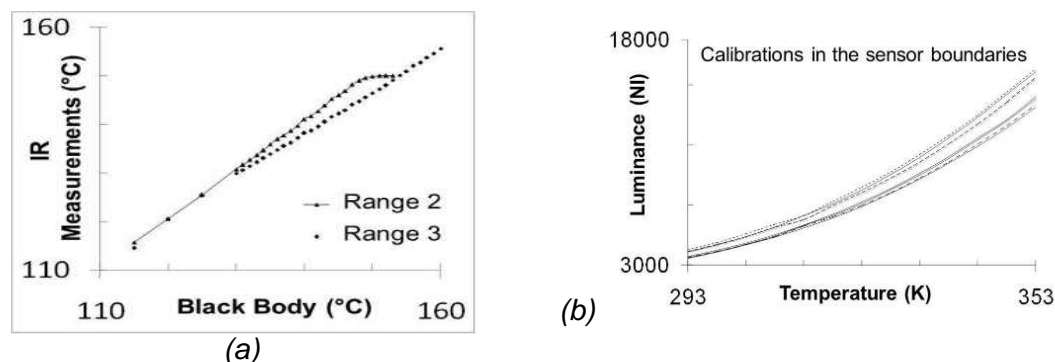

Figure 5.12.   Check of the calibration using an extended black body: (a) Comparison between two ranges of a single camera (FLIR SC1000), (b) Comparison between several pixels responses (CEDIP IRC 320-4LW) of the array.

If the specifications on the measurement accuracy are more stringent than one Kelvin, or if the independence of the measurement is a critical parameter for the later data processing, another solution is to be found. The most logical one consists in performing a customized calibration of the whole sensor matrix with testing conditions and camera configuration (integration time, windowing, etc.) similar to those used for the application, fitting the behavior of each detector independently.

This calibration overcomes the limitations inherent to the NUC (or CNUC) and BPR procedures (linearity assumption valid further enough from saturation for the NUC, introduction of a strong spatial correlation between neighbouring pixels for the BPR operation…). However, it requires a high-uniformity extended blackbody so as to have a uniform radiation source at different temperature levels covering the whole range of the future application.

Once more, as in the standard global calibration procedure, the calibration law of each pixel can be chosen as a polynomial or as a Planck-like function, but the constant will be arrays of coefficients, the size of which being the one of the infrared matrix itself. These calibration coefficients are obtained by approximating, generally in the least squares sense, the couples (digitized radiation–temperature) by the chosen calibration function.

Defective pixels are then localized using a criterion for measuring the mismatch between the calibrated and specified temperature. The BPR operation is not performed: temperatures of the defective pixels are not taken into account in the subsequent data-processing. A specific pixel-to-pixel calibration is detailed in [54].

5.2.   Temporal analysis

Lecture 5: Measurements without contact in heat transfer: page 28

The integration time is the duration during which the radiation coming from the thermal scene is collected by the detectors of the camera. Consequently, it determines the ultimate temporal resolution of the device. As the image transfer time to the storage memory or to the hard disk is often much higher than the integration time (several milliseconds compared to some tenths or hundreds of microseconds), the camera thus does not see the scene during most of the time, which is particularly penalizing for observing fast phenomena.

Regardless of the problems connected to the integration time, the temporal analysis can be disturbed by the absence of some images in the stored sequence. Depending on the devices, a temporal shift of one or two images can occur at the beginning of the sequence. This is due to the fact that the first stored image corresponds to the one that was captured when the starting order occurred, not the actual image at the beginning of the sequence; sometimes, due to pre-processing, the temporal shit can be of two images. Then, on condition that the user is aware of this fact, a simple sequence shift is enough to correct this edge effect.

The second, more penalizing, problem is the absence of some images within a sequence. This problem is relatively unimportant in terms of visualization, but can become critical in the data processing when time is highly involved. Algorithms that are compatible with variable acquisition frequencies are then required. To count and isolate times from the missing images, it is possible to directly read time information in the files from the camera, provided that they have been accurately stored, i.e. sufficient with respect to the acquisition frequencies used. Depending on the camera model, the number of images missing can thus range from one to several dozens.
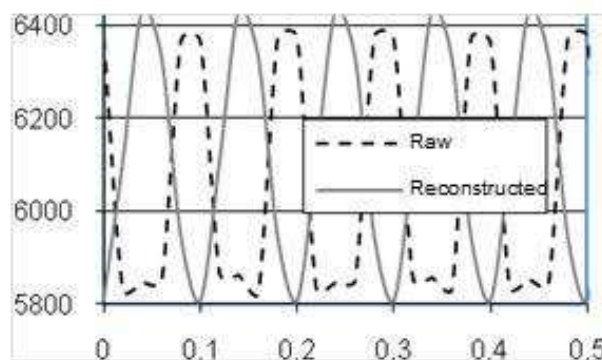

Figure 5.13. Errors induced by the missing images in lock-in thermography: amplitude is not really affected but phase is strongly distorted

Figure 5.13 presents the artefacts observed in the case of a numerical lock-in procedure applied to a series of 500 images in which only two images are missing. If the amplitude is not very affected, the phase has a completely erratic behaviour, and takes a value that depends directly on the number and the phase of the missing images.

5.3.   Spatial resolution

The focal plane array technology has indubitably led to improvements in image quality (Figure 5-4). However, the quality of an image can be considered either from the point of view of the esthetics, or from the one of the metrology. Unfortunately, these two approaches are rarely compatible…
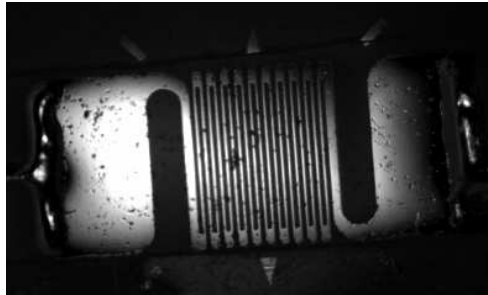

Figure 5.14. Strain gauge (tracks of approximately 20 µm) observed with an "M1" lens.

In order to ensure to obtain reliable measurements, the independence of each sensor relatively to its neighbors must be checked. One of the most current tests for characterizing such equipment is the Slit Response Function (SRF) test: the camera focuses on a thermal side-cooled slit of variable width, placed in front of a hot plate; the following contrast function is then studied:

$$FRF = \frac{V(x) - V_{min}}{V_{max} - V_{min}}, \tag{5.58}$$

where $V(x)$ is the value recorded for a slit width equal to x, V_{max} is the value recorded when the slit is wide open ($x \to \infty$) and V_{min} is the recorded value on the cooled part (Figure 16-5a). In general, it is assumed that, for 320 x 240 pixel cameras, to obtain a good measurement the object must be projected on at least two detectors. Thus, with a lens magnification of 1 ("M1") and a matrix periodicity of 30 µm, one obtains truly independent information only at each step of 60 µm.

A study of this SRF for different positions clearly shows (Figure 5.15) that the pixels are quite more correlated on the edges of the array than in the center. Note that there is indeed a problem of correlation between close measurement points, i.e. on the one hand, only the contrast (and by no means the average value) is affected and, on the other hand, there is convolution of the thermal scene by this response function. Consequently, a simple geometrical correction (e.g. of repositioning of the points in the image, or amplification and/or offsets applied to each pixel) is necessary to recover the real quantitative image of the scene, in addition to a deconvolution procedure.
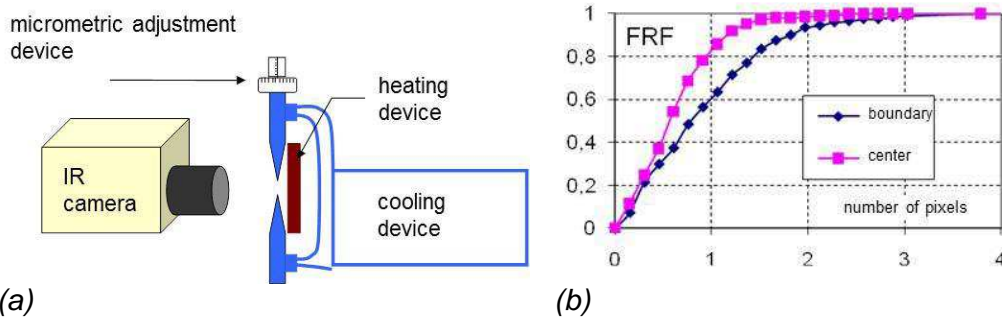
(a)   *(b)*

Figure 5.15. (a) Slit Response Function; (b) SRF near the edge of the array compared to SRF at the centre (CEDIP IRC 320-4 LW camera)

5.4.   Thermal noise and thermal drift

The infrared devices usually used in R&D are cooled at approximately 80 K in order to reduce radiation in the vicinity of the infrared sensors. In new-generation IR cameras, a Stirling cycle engine has replaced liquid nitrogen cooling systems of older cameras. Though the cameras have thus gained in portability, this new system has a non-negligible drawback: the cooling, which was quasi-instantaneous with nitrogen, now requires at least 10 min before any measurement is possible (figure 5.16a).
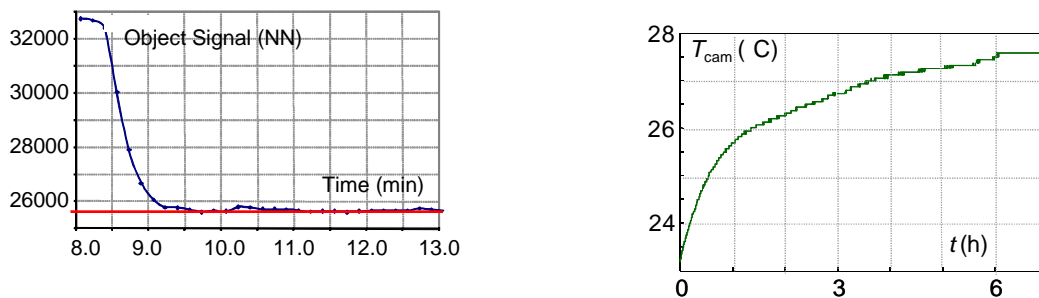

Figure 5.16. (a) Cooling CEDIP IRC320-4LW, (b) thermal drift CEDIP JADE III

In addition, once the cooling is achieved, a slow drift of about 1 to 5 mK per second can occur with certain materials, sometimes over durations reaching a few hours (figure 5.16b). This temperature drift is mainly due to the evolution of the internal temperature of the camera, and modify the sensor responses, so it is appropriate in several situations to wait until the camera temperature is stabilized, or to take this internal drift into account in the conversion of the digitized signal into temperature (Compensated NUC). In addition, certain lower quality materials have instabilities of 0.5 or even 1 K, which that is incompatible with quantitative measurements.

Environment thermal stability

The signal measured by a camera comes primarily from the object (assumed to be gray and opaque in the camera's spectral range), but also, to a lesser extent (in the most favorable conditions), from the environment and atmosphere (figure 5.17). If the environment can be considered as an integral radiator of temperature T_{env} and if the atmosphere between the

target and the camera is isothermal at the temperature T_{atm}, considering a coefficient of transmission τ_{atm}, the measured intensity L_{mes} can be formulated as a function of the intensity L^0 of a blackbody at the object temperature:

$$L_{\text{mes}} = \tau_{\text{a}}.\varepsilon.L^0(T_{\text{obj}}) + \tau_{\text{a}}(1-\varepsilon)L^0(T_{\text{env}}) + (1-\tau_{\text{a}})L^0(T_{\text{atm}})$$

(5.59)

This equation shows that the environment must be reasonably well controlled in order to limit the influence of parasitic radiation (reflection from a radiator or any other radiative IR source, or even from the operator!). This precaution is all the more important when the measured temperature increases are minor. In addition, using a high emissivity coating (thus of low reflectivity) is obviously advantageous to minimize the parasitic flow/object flow ratio.

Along the same lines, note also the presence of the Narcissus effect (reflection of the cold detector on the scene), which is often observed when using a macro lens (e.g. lens magnification of 1, [55]). Usually, this is only an offset map which is superimposed on the scene, and which can thus be offset by subtraction of a reference image.
Last but not least, possible environmental instabilities could modify the exchange conditions between the sample and its environment and thus must be taken into account, especially when there are marked temperature variations over time.

6. Conclusion

Accurate temperature measurement by radiative means is not an easy task. Many parameters have to be evaluated beforehand for extracting the surface emitted radiance from the measured radiance (atmospheric contributions: self-emission and attenuation, environments radiance reflections). One then faces the problem of temperature-emissivity separation. This underdetermined problem requires that some knowledge about the emissivity of the tested material is introduced. A general thought is that by adding spectral measurements at one or several other wavelengths would help identifying the temperature. The underdetermined nature of the problem is however maintained. Introducing a model for the emissivity spectral profile is often a misleading idea: high systematic errors unavoidably emerge when the model doesn't perfectly match to the real emissivity profile. Having some knowledge on emissivity *magnitude* helps much than imposing an arbitrary *shape* model.

7. References

[1]   Siegel R and Howell J R 1972 *Thermal Radiation Heat Transfer* (McGraw Hill).

[2]   Krapez J-C 2011 Radiative measurements of temperature in *Thermal Measurements and Inverse Techniques* (Taylor & Francis)

[3]   Loarer T., Greffet J.-J. and Huetz-Aubert, M. 1990 Noncontact surface temperature measurement by means of a modulated photothermal effect, *Appl. Optics* **29**(7) 979-987

[4]   Loarer T., Greffet J.-J. 1992 Application of the pulsed photothermal effect to fast surface temperature measurements, *Appl. Optics* **31**(25) 5350-5358

[5]   Touloukian Y S and DeWitt D P 1970 *Thermal radiative properties. Thermophysical properties of matter* (Plenum Corp. New-York)

[6]   Salisbury J W and d'Aria D M 1992 Emissivity of terrestrial materials in the 8-14 μm atmospheric window *Remote Sens. Environ.* **42** 83-106

[7]   Baldridge A M, Hook S J, Grove C I and Rivera G 2009 The ASTER Spectral Library Version 2.0 *Remote Sens. Environ.* **113** 711-715 http://speclib.jpl.nasa.gov/

[8]   Corwin R R and Rodenburgh A 1994 Temperature error in radiation thermometry caused by emissivity and reflectance measurement error *Applied Optics* **33**(10) 1950-1957

[9]   Hervé P and Sadou A 2008 Determination of the complex index of refractory metals at high temperatures: application to the determination of thermo-optical properties *Infrared Physics & Technology* **51** 249–255

[10] Pierre T, Rémy B and Degiovanni A 2008 Microscale temperature measurement by the multispecrtral and statistic method in the ultraviolet-visible wavelengths *J. Appl. Phys.* **103** 034904-1-10

[11] Duvaut T, Georgeault D and Beaudoin J L 1996 Pyromètre multispectral infrarouge : application aux métaux *Rev. Gen. Therm* **35** 185-196

[12] Hernandez D, Sans JL, Netchaieff A, Ridoux P, Le Sant V 2009 Experimental validation of a pyroreflectometric method to determine the true temperature on opaque surface without hampering reflections *Measurement* **42** 836-843

[13] Krapez J-C, Bélanger C and Cielo P 1990 A double-wedge reflector for emissivity enhanced pyrometry *Meas. Sci. Technol* **1** 857-864

[14] Foley G.M. 1978 *High Temp. High Press.* **10**:391

[15] Watari M. Watanabe Y., Chigira S., Tamura Y., *Yokogawa Tech. Rep.* **29**:25

[16] Anderson 1985 *Adv. Instrument.* **40**:1337

[17] Tsai B.K., Shoemaker R.L., DeWitt D.P., Cowans B.A., Dardas Z., Delgass W.N., Dail G.J. 1990 Dual Wavelength radiation thermometry: emissivity compensation algorithms, *Int. J. Thermophysics* **11**(1) 269-281

[18] Gardner J L 1980 Computer modelling of a multiwavelength pyrometer for measuring true surface temperature *High Temp – High Press.* **12** 699-705

[19] Coates P B 1981 Multiwavelength pyrometry *Metrologia* **17** 103-109

[20] Hunter B, Allemand C D and Eager T W 1985 Multiwavelength pyrometry: an improved method *Opt. Eng.* **24**(6) 1081-1085

[21] Hunter B, Allemand C D and Eager T W 1986 Prototype device for multiwavelength pyrometry *Opt. Eng.* **25**(11) 1222-1231

[22] Hiernault J P, Beukers R, Heinz W, Selfslag R, Hoch M and Ohse R.W. 1986 Submillisecond six-wavelength pyrometer for high temperature measurements in the range 2000K-5000K *High Temp – High Press.* **18** 617-625

[23] Nordine P C 1986 The accuracy of multicolour optical pyrometry *High Temp. Sci.* **21** 97-109

[24] DeWitt D P and Rondeau R.E. 1989 Measurement of surface temperatures and spectral emissivities during laser irradiation *J. Thermophysics* **3**(2) 153-159

[25] Tank V and Dietl H 1990 Multispectral infrared pyrometer for temperature measurement with automatic correction of the influence of emissivity *Infrared Physics* **30**(4) 331-342

[26] Khan MA, Allemand C and Eager TW 1991 Noncontact temperature measurement. I. Interpolation based techniques *Rev. Sci. Instrum* **62**(2) 392-402

[27] Khan MA, Allemand C and Eager TW 1991 Noncontact temperature measurement. II. Least square based techniques Rev. Sci. Instrum **62**(2) 403-409

[28] Gathers G.R. 1991 Analysis of multiwavelength pyrometry using nonlinear least square fits and Monte Carlo methods *11th Symp. Thermophysic. Prop.* Boulder June 1991

[29] Lindermeir E, Tank V and Hashberger P 1992 Contactless measurement of the spectral emissivity and temperature of surfaces with a Fourier transform infrared spectrometer *Proc. SPIE* 1682 354-364

[30] Duvaut T, Georgeault D and Beaudoin JL 1995 Multiwavelength infrared pyrometry: optimization and computer simulations *Infrared Phys.& Technol.* **36** 1089-1103

[31] Chrzanowski K and Szulim M 1998 Measure of the influence of detector noise on temperature measurement accuracy for multiband infrared systems *Applied Optics* **37**(22) 5051-5057

[32] Chrzanowski K and Szulim M 1998 Error on temperature measurement with multiband infrared systems *Applied Optics* **38**(10) 1998-2006

[33] Chrzanowski K and Szulim M 1999 Comparison of temperature resolution of single-band, dual-band and multiband infrared systems *Applied Optics* **38**(13) 2820-2823

[34] Scharf V, Naftali N, Eyal O, Lipson S G and Katzir A 2001 Theoretical evaluation of a four-band fiber-optic radiometer *Appl Opt.* **40**(1) 104-111

[35] Mazikowski A and Chrzanowski K 2003 Non-contact multiband method for emissivity measurement *Infrared Phys. & Technol.* **44** 91-99

[36] Cassady L D and Choueiri E Y 2003 High Accuracy Multi-color Pyrometry for High Temperature Surfaces *IEPC-03-79 28th Int. Electric Propulsion Conference* Toulouse France March 17-21 2003

[37] Wen C D and Mudawar I 2004 Emissivity characteristics of roughened aluminium alloy surfaces and assessment of multispectral radiation thermometry (MRT) emissivity models *Int. J. Heat Mass Transfer* **47** 3591-3605

[38] Wen C D and Mudawar I 2004 Emissivity characteristics of polished aluminium alloy surfaces and assessment of multispectral radiation thermometry (MRT) emissivity models *Int. J. Heat Mass Transfer* **48** 1316-1329

[39] Sade S and Katzir A 2004 Multiband fiber optic radiometry for measuring the temperature and emissivity of gray bodies of low or high emissivity *Appl. Opt.* **43**(9) 1799-1810

[40] Uman I and Katzir A 2006 Fiber-optic multiband radiometer for online measurements of near room temperature and emissivity *Optic Letters* **31**(3) 326-328

[41] Duvaut T 2008 Comparison between multiwavelength infrared and visible pyrometry: application to metals *Infrared Phys.& Technol.* **51** 292-299

[42] Rodiet C, Rémy B, Degiovanni A and Demeurie F 2013 Optimisation of wavelengths selection used for the multi-spectral temperature measurement by ordinary least squares method of surfaces exhibiting non-uniform emissivity *Quantitative InfraRed Thermography Journal* **10**(2) 222-236

[43] Barducci A and Pippi I 1996 Temperature and emissivity retrieval from remotely sensed images using the "grey body emissivity" method *IEEE Trans. Geosci. & Remote Sensing* **34**(3) 681-695

[44] Gardner J L, Jones T P, Davies M R 1981 A six wavelength pyrometer, *High Temp – High Press.* **13** 459-466

[45] Gillespie A., Rokugawa S., Matsunaga T., Cothern J.S., Hook S., Kahle A.B. 1998 A temperature and emissivity separation algorithm for advanced spaceborne thermal emission and reflection radiometer (ASTER) images, *IEEE Trans. Geosci. Remote Sens.* **36**(4): 1113-1126

[46] Sabol D.E., Gillespie A.R., Abbott E., Yamada G. 2009 Field validation of the ASTER temperature and emissivity separation algorithm, *Remote Sens. Environ.* 113: 2328-2344

[47] Oltra-Carrio R., Cubero-Castan M., Briottet X., Sobrino J. Analysis of the performance of the TES algorithm over urban areas *IEEE Trans. Geosci. Remote Sens.* 52(11)6989-6998

[48] Gaussorgues G, « La Thermographie Infrarouge - Principes, Technologie, Applications », 4ème Édition, Tec & Doc Lavoisier, 1999.

[49] Pajani D, « Mesure Par Thermographie Infrarouge », Editeur ADD, EAN13 9782950417107, 1989.

[50] Pron H, Menanteau W, Bissieux C, Beaudoin JL, "Characterization of a focal plane array (FPA) infrared camera", QIRT 2000 (Eurotherm No. 64), Reims, 18-21 juillet 2000, pp 112-117

[51] Bissieux C, Pron H et Henry J-F "Pour de véritables caméras matricielles de recherche", revue Contrôles Essais Mesures, janvier 2003, vol n°2, pp. 39-41

[52] Pron H, Laloue P, Henry J-F, L'ecolier J, Bissieux C et Nigon F, "Caractérisation de caméras infrarouges à matrice de détecteurs", 3ème Colloque Interdisciplinaire en Instrumentation, ENS Cachan, 29-30 janvier 2004, vol. 2, pp. 215-222.

[53] Pron H and Bissieux C, "Focal Plane Array infrared cameras as research tools", QIRT Journal, Vol 1/2 (2004), pp 229-240

[54] Honorat V, Moreau S, Muracciole J-M, B. Wattrisse B, Chrysochoos A, « Calorimetric analysis of polymer behaviour using a pixel calibration of an IRFPA camera », *Int J. on Quantitative IR Thermography*, 2, (2), pp.153-172, 2005.

[55] Poncelet M, Witz J-F, Pron H, Watrisse B, "A study of IRFPA camera measurement errors: radiometric artefacts", QIRT Journal. Vol. 8 N° 1/2011, pp 3-20